The Journal of Clinical Endocrinology & Metabolism, 2022, Vol. 107, No. 3, 755–775
https://doi.org/10.1210/clinem/dgab756
Clinical Research Article

Clinical Research Article

Proteomic Signatures of Human Visceral and Subcutaneous Adipocytes

Pavel Hruska,[1,2,3,*] Jan Kucera,[3,*] Matej Pekar,[4,5] Pavol Holéczy,[4,6] Miloslav Mazur,[4] Marek Buzga,[7,8] Daniela Kuruczova,[3] Peter Lenart,[3] Jana Fialova Kucerova,[1] David Potesil,[2] Zbynek Zdrahal,[2] and Julie Bienertova-Vasku[1,3]

[1]Department of Pathological Physiology, Faculty of Medicine, Masaryk University, 62500 Brno, Czech Republic; [2]Central European Institute of Technology, Masaryk University, 62500 Brno, Czech Republic; [3]Research Centre for Toxic Compounds in the Environment, Faculty of Science, Masaryk University, 62500 Brno, Czech Republic; [4]Department of Surgery, Vitkovice Hospital, 70300 Ostrava, Czech Republic; [5]Department of Physiology, Faculty of Medicine, Masaryk University, 70300 Brno, Czech Republic; [6]Department of Surgical Disciplines, Faculty of Medicine, University of Ostrava, 70300 Ostrava, Czech Republic; [7]Department of Human Movement Studies, Faculty of Education, University of Ostrava, 70900 Ostrava, Czech Republic; and [8]Department of Physiology and Pathohysiology, Faculty of Medicine, University of Ostrava, 70300 Ostrava, Czech Republic

ORCiD number: 0000-0003-0705-854X (P. Hruska); 0000-0001-5327-808X (J. Bienertova-Vasku).

*Co-first/equal authorship: P.Hr. and J.K. contributed equally to the manuscript.

Abbreviations: BMI, body mass index; DMEM/F12, Dulbecco's Modified Eagle Medium/Nutrient Mixture F12; DXA, dual-energy x-ray absorptiometry; ECM, extracellular matrix; ERAD, endoplasmic reticulum-associated degradation; FDR, false discovery rate; FFA, free fatty acid; GO, gene ontology; GS, gene significance; HDL, high-density lipoprotein; LC-MS, liquid chromatography-mass spectrometry; LDL, low-density lipoprotein; LPL, lipoprotein lipase; MS, mass spectrometry; OXPHOS, oxidative phosphorylation; SA, subcutaneous adipocytes; SAT, subcutaneous adipose tissue; SDS, sodium dodecyl sulfate; UA (buffer), 8M urea in 0.1M Tris/HCl; VA, visceral adipocytes; VAT, visceral adipose tissue; WGCNA, weighted gene co-expression network analysis.

Received: 21 May 2021; Editorial Decision: 13 October 2021; First Published Online: 20 October 2021; Corrected and Typeset: 19 November 2021.

Abstract

Context: Adipose tissue distribution is a key factor influencing metabolic health and risk in obesity-associated comorbidities.

Objective: Here we aim to compare the proteomic profiles of mature adipocytes from different depots.

Methods: Abdominal subcutaneous (SA) and omental visceral adipocytes (VA) were isolated from paired adipose tissue biopsies obtained during bariatric surgery on 19 severely obese women (body mass index > 30 kg/m^2) and analyzed using state-of-the-art mass spectrometry. Differential expression analysis and weighted gene co-expression

ISSN Print 0021-972X ISSN Online 1945-7197
Printed in USA

network analysis (WGCNA) were performed to investigate proteome signature properties and to examine a possible association of the protein expression with the clinical data.

Results: We identified 3686 protein groups and found 1140 differentially expressed proteins (adj. *P* value < 0.05), of which 576 proteins were upregulated in SA and 564 in VA samples. We provide a global protein profile of abdominal SA and omental VA, present the most differentially expressed pathways and processes distinguishing SA from VA, and correlate them with clinical and body composition data. We show that SA are significantly more active in processes linked to vesicular transport and secretion, and to increased lipid metabolism activity. Conversely, the expression of proteins involved in the mitochondrial energy metabolism and translational or biosynthetic activity is higher in VA.

Conclusion: Our analysis represents a valuable resource of protein expression profiles in abdominal SA and omental VA, highlighting key differences in their role in obesity.

Key Words: adipose tissue, visceral adipose tissue, subcutaneous adipose tissue, obesity, adipocytes, metabolism

Adipocytes, the major adipose tissue cell type, are essential for their physiological and pathophysiological processes, which include energy storage and release, metabolic homeostasis, and immune response regulation (1). They store energy in the form of triglycerides, predominantly in 2 anatomical depots: visceral and subcutaneous (2). Both sites share similar properties; however, the functional differences between subcutaneous adipose tissue (SAT) and visceral adipose tissue (VAT) with respect to insulin sensitivity, fatty acid composition, and bioactive molecule secretion are critical to health outcomes (3). Especially in the context of obesity, evidence supports a distinct pathological contribution related to the anatomical location of adipose tissue (4). Hence, SAT is generally considered metabolically less detrimental in comparison with VAT, which is strongly associated with the risk of cardiovascular disease, diabetes, cancer, and other comorbidities (5, 6). However, detailed molecular features related to the functional differences of adipose depots remain obscure. In particular, little is known about alterations at the protein level.

Developments in proteomics technology provide us with a powerful tool for identifying the differences between the adipose tissue depots and enable us to reveal cell-specific expression patterns (7). While the human adipose proteome has already been investigated, studies are significantly limited by intrinsic adipose tissue heterogeneity (8-11), a lack of comparing different depots (12, 13), or a reliance on a targeted approach limited to monitoring only selected proteins (14). To overcome these issues, we used isolated mature adipocytes from paired SAT and VAT biopsies from 19 morbidly obese female subjects (body mass index [BMI] ~ 40) and performed label-free comparative liquid chromatography-mass spectrometry (LC-MS) suitable for in-depth proteome analysis.

Our goal was to characterize the proteomic features of SAT and VAT adipocytes and their potential contribution to the function of adipose tissue in obesity. By employing the combination of the extreme phenotype of our cohort, which further amplifies differences between adipose locations, and state-of-the-art proteomics, our study unveiled complex depot-specific profiles of isolated adipocytes. This is, to date, the most comprehensive proteomic analysis of adipocytes, newly highlighting the distinct role of each depot in obesity and thus advancing our understanding of adipocyte biology.

Methods

Patients

This study included 19 women (mean age = 47 ± 8 years, obesity grade II and III, BMI = 41.32 ± 4.23 kg/m^2) who underwent bariatric/metabolic surgery at the Department of Surgery, Vitkovice Hospital, Ostrava. Patient selection followed the guidelines of the International Federation for the Surgery of Obesity (IFSO) (www.ifso.com/body-mass-index). All patients were white of Central European origin, 10 suffered from arterial hypertension, 5 from hyperlipidemia, 3 from type II diabetes, 4 from asthma. The study originally included 20 women and 4 men; however, the male samples were underrepresented and thus excluded from the study—data available at the PRIDE repository (15). One female patient was excluded due to the outlying data pattern of visceral adipocyte protein intensities.

Anthropometric assessment (body weight, height, waist, and hip circumference) was performed prior to surgery. Dual-energy x-ray absorptiometry (DXA) measurements were performed to determine body composition and body fat distribution using a Hologic densitometer (Discovery

A; Hologic, Waltham, MA, USA) calibrated according to the manufacturer's recommendations. The precision error of the densitometer and coefficient of variation were established, and the value of the least significant change was calculated as described in previous studies (16-18). Fasting blood glucose, cholesterol, triglycerides, high-density lipoprotein (HDL), low-density lipoprotein (LDL), and glycated hemoglobin A1c (HbA1c) concentrations were also measured prior to surgery. The characteristics of the participants are shown in Table 1.

All patients signed written informed consent before participation in the study and the design of the study was approved by the Multicentric Ethics Committee of Vitkovice Hospital, Ostrava (No. EK/3/17) according to the principles of the Declaration of Helsinki.

Adipocyte Isolation and Culture

SAT was obtained from the subcutaneous abdominal area between the xiphoid process and umbilicus on the left side of the patient. The incision was then used as a laparoscopic port and all procedures were performed laparoscopically in the standard manner as described in previous studies (19, 20). VAT was taken from the front part of the omentum majus. Utilized bariatric procedures included laparoscopic greater curvature plication (LGCP), laparoscopic sleeve gastrectomy (LSG), and Roux-en-Y gastric bypass (RYGB). The type of surgery did not influence the manner of adipose tissue biopsy.

Obtained biopsies were placed into a tube with 20 mL of Dulbecco's Modified Eagle's Medium/Nutrient Mixture F-12 Ham (DMEM/F12, Sigma-Aldrich, Cat# D6421) and transferred at room temperature for adipocyte isolation. The following procedures were carried out under a laminar flow hood using sterile equipment. Adipocytes were isolated using a previously described method (21), briefly stated here: adipose tissue was washed 3 times with sterile phosphate-buffered saline (PBS) and visible blood veins were removed from samples. After being minced into approximately 10-mg fragments using scissors, the tissue was digested with Standard Grade NB 4 Collagenase (Serva, Cat# 1745401), 1 mg/mL in DMEM/F12 for 2 hours at 37 °C with shaking (100 rpm). The enzymatic reaction was stopped by adding DMEM/F12 supplemented with 10% fetal bovine serum (FBS, Biosera, Cat# 1001). The mixture was filtered through a 500 µm plastic mesh and centrifuged at 300*g* for 5 minutes. This step was repeated twice. Floating adipocytes were then collected, washed twice in DMEM/F12, and seeded in a T75 flask in DMEM/F12 supplemented with 10% FBS. The cells were allowed to recover overnight before they were washed 3 times in PBS and frozen at −80 °C.

Table 1. Description of participants

	Mean ± SD
Age, years	47 ± 8
Height, cm	164 ± 4
BMI, kg/m^2	41.32 ± 4.23
Waist1, cm (inferior margin of the ribs)	110 ± 9
Waist2, cm (umbilical level)	125 ± 12
Hip, cm	130 ± 9
Waist1 to hip ratio	0.84 ± 0.04
Waist2 to hip ratio	0.96 ± 0.07
DXA	
Body weight, kg	112 ± 12
Lean mass, kg	56 ± 5
Body fat mass, kg	53 ± 8
Visceral fat mass, g	1001 ± 236
Visceral fat volume, cm^3	1082 ± 255
Visceral fat area, cm^2	208 ± 49
Android to gynoid ratio	1.07 ± 0.09
Fat mass index, kg/m^2	30 ± 3
Lean mass index, kg/m^2	21 ± 1
Clinical laboratory data	
Glycemia, mmol/L	5.9 ± 0.9
Cholesterol, mmol/L	5.3 ± 0.7
Triglycerides, mmol/L	2.1 ± 0.9
HDL, mmol/L	1.2 ± 0.2
LDL, mmol/L	3.4 ± 1.0
HbA1c, mmol/L	3.9 ± 0.4

The table shows average body composition and clinical data of the 19 women included in this study before the bariatric surgery.
Abbreviations: BMI, body mass index; DXA, dual-energy x-ray absorptiometry; HbA1c, glycated hemoglobin A1c; HDL, high-density lipoprotein; LDL, low-density lipoprotein.

Protein Extraction and On-Filter Digestion

All adipocyte samples were completely thawed and vortexed with an SDT lysis buffer (4% sodium dodecyl sulfate [SDS; Sigma-Aldrich, Cat# 436143], 0.1 M dithiothreitol [DTT; Thermo Fisher Scientific, Cat# R0862], 0.1 M Tris/HCl [Sigma-Aldrich, Cat# 10812846001], pH = 7.6) in a Thermomixer® (Eppendorf) for one minute. The mixtures were subsequently heated at 95 °C for 30 minutes while mixing at high speed. The supernatant was cleared by centrifugation (20 000*g*, 15 minutes) and the solution below the lipid layer was collected for further processing. Protein extract quality and its concentration were assessed by 1D SDS-PAGE (22) to ensure comparable conditions for all samples during filter-aided sample preparation (FASP) (23, 24). Protein lysates (50 µg) were mixed with 8M UA buffer (8M urea [Sigma-Aldrich, Cat# U1250] in 0.1M Tris/HCl [Sigma-Aldrich, Cat# 10812846001], pH 8.5) on Microcon-30 kDa cutoff filters (Merck Millipore, Cat# MRCF0R030) and centrifuged at 14 000*g* for 30 minutes at 20 °C. The retained proteins were washed with 200 µL UA buffer. The final protein precipitate in the Microcon

devices was mixed with 100 µl of UA buffer containing 50mM iodoacetamide (Sigma-Aldrich, Cat# I1149) and incubated in the dark for 20 minutes at room temperature. Subsequently, the samples were washed 3 times with 100 µL UA buffer and 3 times with 100 µL of 50 mM NH_4HCO_3 (Sigma-Aldrich, Cat# A6141). Finally, trypsin (enzyme:protein ratio of 1:50; sequencing grade, Promega, Cat# V5111) was added onto the filter and the mixture was incubated for 18 hours at 37 °C. The tryptic peptides were then eluted by centrifugation followed by 2 additional elution steps with 50 µL of 50 mM NH_4HCO_3. Peptides were then cleaned by liquid-liquid extraction (3 iterations) using water-saturated ethyl acetate (25). Cleaned filter-aided sample preparation eluates were evaporated completely in a SpeedVac concentrator (Thermo Fisher Scientific). The resulting peptides were extracted into LC-MS vials by 2.5% formic acid (FA) in 50% acetonitrile and 100% acetonitrile with an addition of polyethylene glycol (20 000; final concentration 0.001 %) (26) and concentrated in a SpeedVac concentrator (Thermo Fisher Scientific). The samples were processed in 2 batches (12 sample pairs per batch).

Liquid Chromatography–Mass Spectrometry

Peptide mixtures were measured using an LC-MS/MS system consisting of an Ultimate 3000 RSLCnano system (SRD-3400, NCS-3500RS CAP, WPS-3000 TPL RS; Thermo Fisher Scientific) combined with an Orbitrap Fusion Lumos system (Thermo Fisher Scientific) with Digital PicoView 550 nanospray ion source. Tryptic digests (~2 µg/injection) were online concentrated and desalted on a trapping column (100 µm × 30 mm, filled with 3.5 µm X-Bridge BEH 130 C18 sorbent (Waters, Milford)) using 0.1% formic acid in water. The peptides were eluted from the trapping column onto an Acclaim Pepmap100 C18 analytical column (3 µm particles, 75 µm × 500 mm; Thermo Fisher Scientific, Cat# 164570). Peptides were separated using a 120-minute gradient (mobile phase A—0.1% formic acid in water; mobile phase B—0.1 % formic acid in 80% (*v/v*) acetonitrile. Peptides were eluted with a linear 75-minute gradient of 1% to 30 % of mobile phase B, followed by a 30-minute increase to 56% of mobile phase B and a 5-minute increase to 80% of mobile phase B, and a 10-minute wash of 80% mobile phase B at a flow rate of 300 nL/min.

Mass spectrometry (MS) data were acquired using data-dependent acquisition. Target values for full scan MS spectra were 4×10^5 charges in *m/z* range 350 to 2000 with a maximum injection time of 54 ms and a resolution of 60 000 at *m/z* 200. MS/MS scans after HCD fragmentation with 30% collision energy were performed at a resolution of 30 000 at *m/z* 200 with an ion target value of 5×10^4 and a maximum injection time of 50 ms. All peptide mixtures were analyzed separately in a randomized manner; VA and SA samples from each patient were analyzed together.

MS Data Analysis

MS raw data files were analyzed using MaxQuant software (v. 1.6.1.0) (27) using default settings unless otherwise noted. MS/MS ion searches were performed against the UniProtKB Human FASTA database (Homo sapiens, taxon ID 9606, version 2018-05 from 28.05.2018) and cRAP contaminant database (version 170518; thegpm.org/crap) using the Andromeda search engine (Cox et al., 2011). Carbamidomethylation on cysteine was set as a fixed modification and N-terminal acetylation, methionine oxidation, and asparagine/glutamine deamination as variable modifications. Trypsin/P enzyme with 2 allowed missed cleavages and minimal peptide length of 6 amino acids were set. The false discovery rate (FDR) was 0.01 for both protein and peptide levels. The match-between-runs algorithm was used across the whole dataset to improve peptide matching. The mass spectrometry proteomics data and the search results have been deposited to the ProteomeXchange Consortium via the PRIDE (15) partner repository with the dataset identifier PXD024734.

Statistical and Bioinformatics Analyses

Protein intensities reported in the proteinGroups.txt file (output of MaxQuant) were further processed using the software container environment (https://github.com/OmicsWorkflows) version 3.7.2a and R software (28). Processing workflow is available upon request. Briefly, it included the following: (a) removal of decoy hits and contaminant protein groups; (b) exclusion of 4 male sample pairs and an outlying sample pair; (c) protein group intensities $\log_2$ transformation; (d) LoessF normalization; and (e) missing values imputation using the imp4p package. Protein groups were only considered for subsequent analysis if they contained measured intensity value in at least 8 samples of VA or SA and were identified to at least 2 peptides. The imputed normalized protein intensities (Supplemental File 1 (29)) were used for differential expression analyses using the LIMMA R package (30). The linear model used to compare paired differences between SA and VA samples was adjusted for batch effect by adding batch number as a variable in the model. The correlation between sample pairs was included in the linear model using appropriate functions from the LIMMA package (31). Subsequently, the results were adjusted for multiple hypothesis testing using the Benjamini and Hochberg procedure (32) implemented in

the LIMMA package. LIMMA test results are provided in Supplemental File 2 (29).

Global correlation analysis was performed on normalized imputed log2-transformed intensity data. Two separate correlation matrices were constructed for SA and VA intensities. The Pearson correlation coefficient was used to calculate the correlations. The correlations were then subtracted from 1, resulting in values in the 0 to 2 range. These values were then used as distances in unsupervised hierarchical clustering using Ward's algorithm (33). The resulting correlation matrices present the correlations ordered into clusters obtained using this method.

The relationship between SA and VA protein expression and clinical traits was assessed using a weighted gene co-expression network analysis (WGCNA) R package (34, 35). The log2-transformed normalized and imputed intensity data was used to construct the biweighted mid-correlation signed co-expression network. The adjacency matrix satisfying the approximate scale-free topology network was used to calculate Topological Overlap Measure, and the corresponding dissimilarity was used to produce a hierarchical clustering tree of proteins. Modules of highly interconnected proteins were defined using the Dynamic Tree Cut of the dendrogram branches, and subsequent merging of highly similar modules. Each module was then assigned a designated color. For each module, an eigengene was defined as the first principal component of the module, and module membership was determined by calculating the Pearson correlation between each module eigengene and each protein, together with corresponding *P* values (36). Module-trait relationships were calculated as Pearson correlations between each module eigengene and clinical traits. Modules with a significant trait correlation *P* value < 0.05 and absolute correlation value > 0.5 were selected for STRING (37) functional enrichment analysis. Hub proteins with the highest module membership and proteins with the most significant trait correlation based on gene significance (GS) values within the selected modules were further investigated in the context of AT and obesity.

Gene ontology (GO) enrichment analyses were performed in Cytoscape 3.8.0 using ClueGO (v. 2.5.7) and the CluePedia (v. 1.5.7) plugin (38) showing only terms where the *P* value < 0.05. The enrichment of biological processes, molecular function and the cellular compartment for the whole adipocyte proteome was set to show the top 2 levels of GO terms. Default search parameters were used for the enrichment of significant proteins. The pathway analyses were performed using the open-source peer-reviewed pathway database Reactome (39) with subsequent pathway visualization using ClueGO + CluePedia including the import of STRING database scores (37) into the network. This approach facilitated the visualization of complex pathway networks with protein-protein interactions among the most differentially expressed proteins between SA and VA.

The prediction of putative secreted proteins was conducted using the SignalP-5.0 Server, enabling the prediction of the secretory signal peptide sequence for transport by the Sec translocon and cleaved by Signal Peptidase I using a deep neural network (40). This analysis was performed using the FASTA sequence of the most differentially expressed proteins with $\log_2 FC > 1$.

Results

Overview of Global Adipocyte Proteome

In this study, we used mature adipocytes derived from abdominal SAT and omental VAT biopsies collected from 19 obese female patients during bariatric surgery. Adipocytes from 2 distinct adipose tissue depots were used for label-free quantitative LC-MS profiling. We generated a dataset of 38 adipocyte proteomes with a total of 3686 identified proteins; we provide this proteome dataset in an easily accessible and minable format for the benefit of the entire community (PRIDE accession PXD024734). In order to minimize the chance of false positivity, we excluded protein groups identified only by a single peptide match, and protein groups quantified in less than 8 of the 19 SA or VA samples for subsequent analysis. The final dataset with 2939 quantified protein groups was used to compare measured intensities in SA and VA samples (Supplemental File 1 (29)). The whole dataset was comparable in the means of identified proteins between the SA and VA. The variability between the replicates was minimal, with Pearson correlation coefficients between measured intensities of (0.81–0.93) for not normalized $\log_2$ transformed data, and (0.83–0.94) for loess normalized $\log_2$ transformed data (data not shown).

First, we annotated the whole proteome with gene ontology (GO) terms and performed an enrichment analysis to describe the proteome structure, and subsequently compared the functional distribution of differentially expressed proteins. The overall adipocytes proteome enrichment analysis showed the distribution of all proteins within the adipocytes' cellular components (CC), biological processes (BP), and molecular function (MF) (Figure 1). The most enriched GO CC terms included cytoplasm, cytosol, extracellular space, and the endomembrane system, as well as inner cell complexes like the mitochondrial protein complex, actin filament bundle, and ribonucleoprotein complex. The most enriched biological processes in our adipocyte proteome are the establishment of localization, small molecule metabolic process, oxidation-reduction process, cellular metabolic process, and cellular component organization

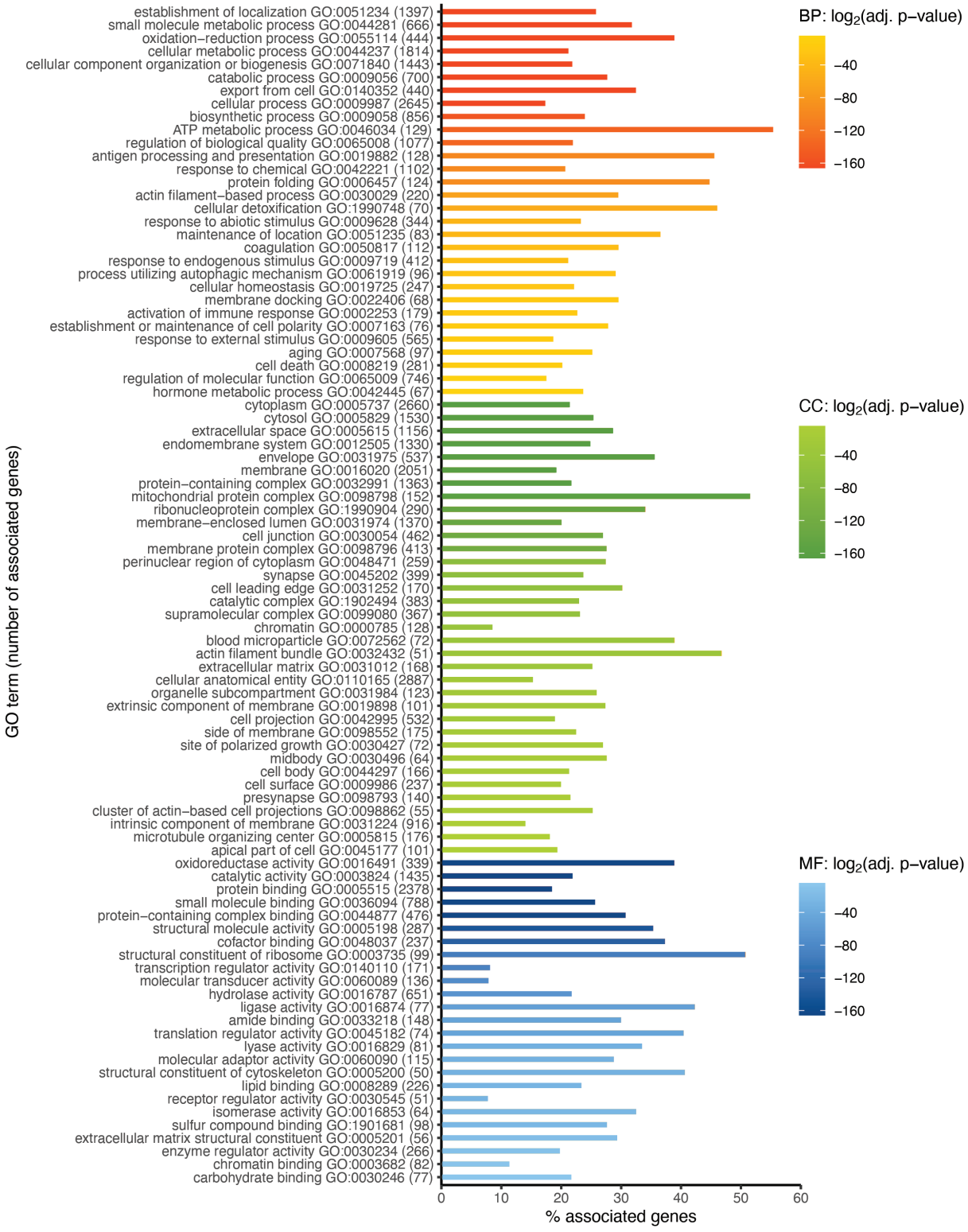

Figure 1. Global proteome GO term enrichment. GO enrichment analysis of all identified proteins (n = 2939) in the SA and VA adipocytes. The enrichment analysis was retrieved using ClueGO limited to top 2 GO term levels for biological processes (BP), cellular components (CC), and molecular function (MF). The figure shows the percentage of associated genes from the adipocyte proteome represented by significantly enriched GO terms (adj. *P* value < 0.05). The GO terms are sorted from the most significant on top to less significant on the bottom for each GO term group, respectively.

or biogenesis. Among others, the ATP metabolic process is also significantly enriched with over 55% of associated genes for a given term. The proteome enrichment analysis based on the molecular function shows mainly catalytic activity, protein binding, small molecule binding, followed by proteins involved in hydrolase activity, oxidoreductase

activity, structural molecule activity, cofactor binding, or lipid binding.

Global Adipocyte Proteome Correlation Maps Reveal Cell-Specific Functional Expression Patterns

Next, we hypothesized that proteins are present in functionally related networks with a close relation to protein abundance levels. Therefore, we used a global correlation map with a pairwise relationship of all 2939 proteins. The cross-correlation of all measured protein intensities generated a matrix of 8 637 721 Pearson's correlation coefficients which were clustered using unsupervised hierarchical clustering into the global correlation map for SA and VA samples respectively. The global correlation maps show distinct expression patterns between SA and VA proteomes. Therefore, the apparent protein clusters were submitted to GO enrichment analysis, and we revealed several functionally related protein clusters in both adipocyte proteomes (Fig. 2A and 2B). Although most of the cellular processes and compartments formed clusters in both proteomes, some clusters were larger with a stronger linear relationship in one of the proteomes than in the other. The SA proteome creates highly correlated clusters enriched especially in peptide metabolic and biosynthesis processes, transport, the establishment of protein localization, extracellular exosome, and vesicular transport. On the other hand, the VA proteome creates a large cluster of strong correlations enriched by proteins of cellular respiration, generation of precursor metabolites and energy, and mitochondrion and clusters involved in lipid metabolic process, as well as protein transport and localization, and peptide metabolic processes.

Bioinformatic Analyses of Differentially Expressed Proteins Reveal Adipocytes' Functional Differences

To reveal differences between SA and VA protein expression, we compared both adipocyte cell lines at protein abundance level. A comparison of the measured protein MS intensity values between VA and SA proteomes revealed 1140 differentially expressed proteins (adj. P value < 0.05) (Supplemental file 2 (29)). Where 576 proteins were upregulated in SA, and 564 in VA samples, respectively. To investigate what biological processes, molecular functions, and cellular components are enriched by the SA and VA upregulated proteins, all significantly upregulated proteins were submitted to ClueGO (v. 2.5.7) with a significance threshold of 0.05 and merging all redundant groups with > 50% overlap. All proteins were annotated based on current knowledge of protein domain molecular-level activities, locations relative to cellular structures, or participation in biological processes, to reveal the major biological differences between SA and VA.

Based on the cellular component enrichment analysis, most of the upregulated proteins in SA are associated with membrane-related terms such as organelle membrane, vesicle, whole membrane, bounding membrane of organelle, etc. In contrast to SA, VA upregulated proteins are enriched mainly by proteins localized to the cytosol, extracellular vesicle, mitochondrion, and mitochondrial respiratory chain complex I (Fig. 3A).

The enrichment analysis of biological processes (Fig. 3B) displayed most of the SA upregulated proteins in the cellular component organization, the establishment of localization in cell, vesicle-mediated transport, response to organic substance, or cellular catabolic process. Generally, the most significantly enriched groups were related to transport activities like vesicle-mediated transport, the establishment of localization in cell or Golgi vesicle transport, but also to metabolic processes associated with lipid metabolism and storage, cellular catabolic processes, or carbohydrate derivative metabolic processes. On the other hand, the most VA upregulated proteins were associated with the organonitrogen compound metabolic process, organelle organization, organic substance catabolic process, cellular catabolic process, or organic acid metabolic process. Taken together, of all enriched groups in VA, the most significant enrichment was observed in metabolic processes, especially in relation to the cellular catabolism including macromolecules and small molecules. Moreover, a significant enrichment was observed in terms related to mitochondrial energy metabolism such as oxidoreductase activity, mitochondrial respiratory chain complex I assembly, electron transport, or generation of precursor metabolites and energy.

In terms of molecular function enrichment analysis (Fig. 3C) SA upregulated proteins showed only a few significantly enriched functional groups in comparison to VA. Here, most of the SA upregulated proteins act in cytoskeletal protein binding, cell adhesion molecule binding, purine ribonucleotide binding, or coenzyme binding. In contrast, the upregulated proteins of VA are functionally enriched, especially in oxidoreductase activity, coenzyme binding, nucleotide binding, or RNA binding.

Pathway Enrichment Analysis Reveals the Most Profound SA and VA Differences

In order to explore processes and pathways enriched by the upregulated proteins in SA and VA respectively, we analyzed the lists of upregulated proteins using the Reactome database. The Reactome database allows

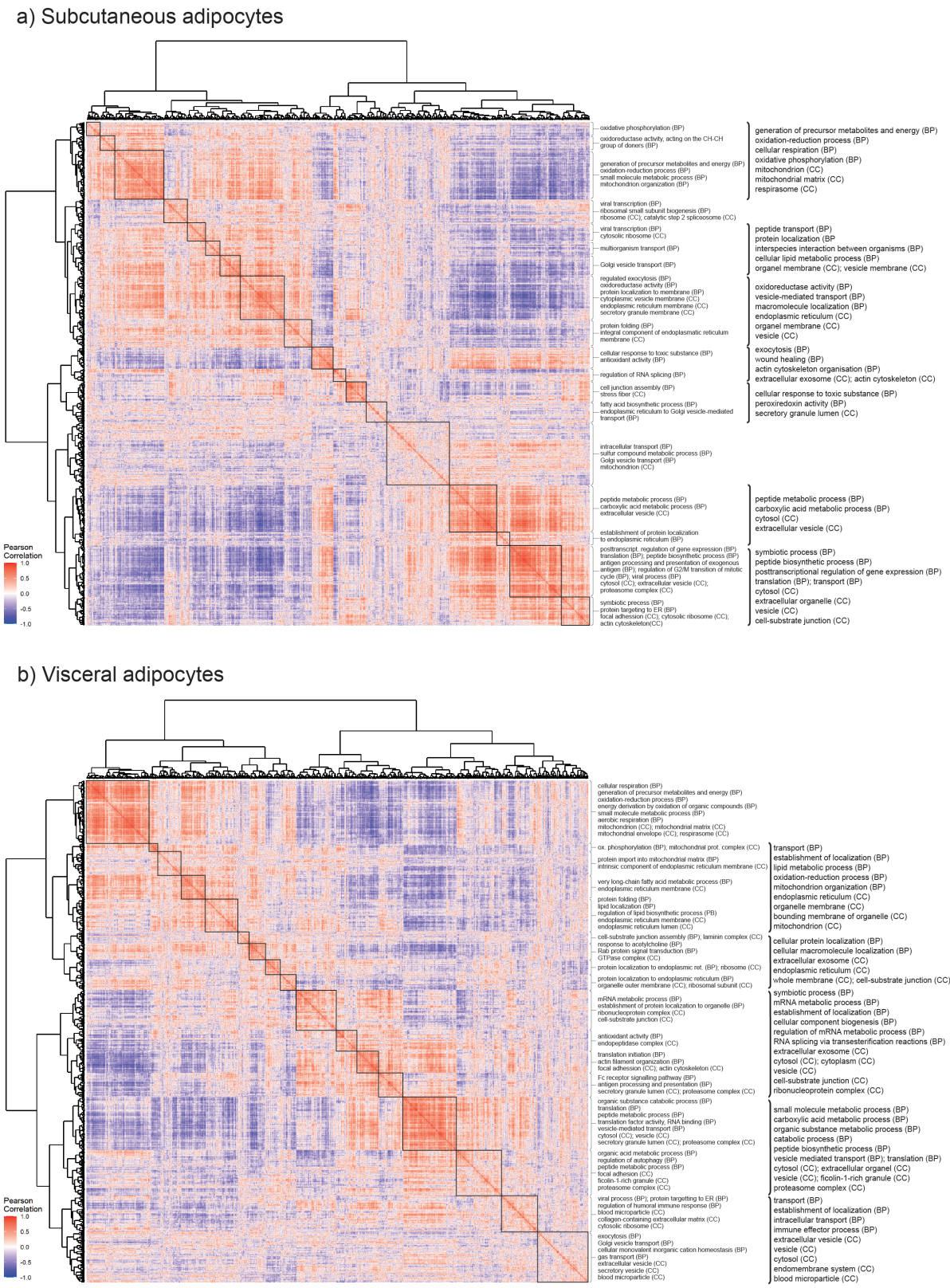

Figure 2. Global correlation map of SA and VA proteome. The global correlation maps show cross-correlations of all quantified proteins using Pearson correlation coefficient and subsequent unsupervised hierarchical clustering for a) SA and b) VA proteome, respectively. This analysis revealed extensive maps of co-regulated proteins in respective clusters. In the map, proteins with a strong correlation or anti-correlation to each other cluster together in red or blue areas, respectively. The protein lists of the main correlation clusters were submitted to ClueGO enrichment analysis of biological processes (BP), and cellular components (CC). The most significantly enriched terms of 2 cluster levels can be found on the right from the maps.

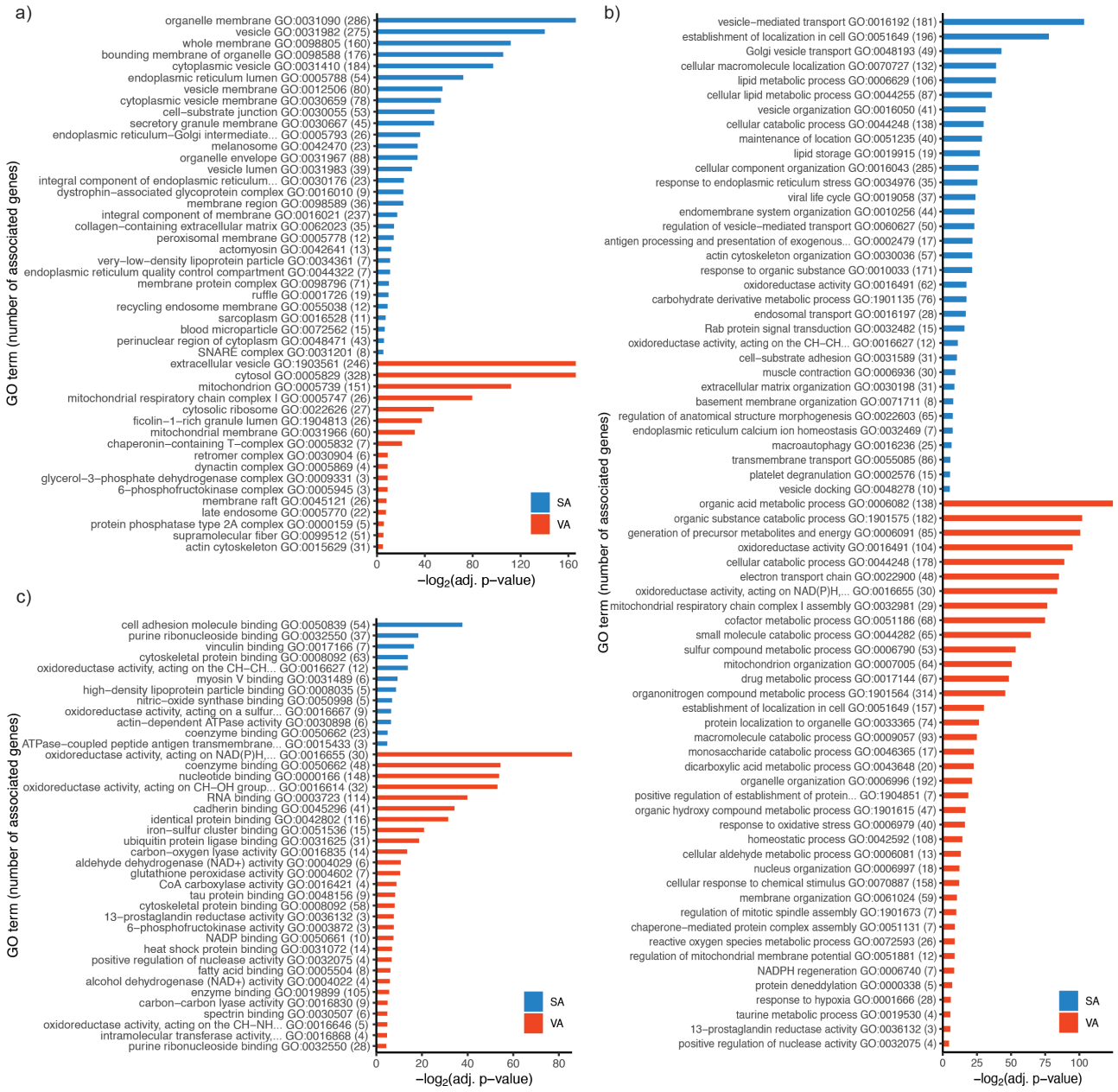

Figure 3. SA and VA GO term enrichment. GO enrichment analysis of all significantly upregulated SA (n = 576) and VA (n = 564) proteins. The enrichment analysis was retrieved using ClueGO with a significance threshold of 0.05 and merging all redundant groups with > 50% overlap for a) cellular components (CC), b) biological processes (BP), and c) molecular function (MF). The figure shows the most significantly enriched GO terms (adj. *P* value < 0.05) for SA, and VA upregulated proteins, respectively.

overrepresentation pathway analysis of curated pathways and reactions in human biology. Reactome pathways are arranged in a hierarchy and the overrepresented pathways score is corrected for false discovery rate using the Benjamini-Hochberg method. This resulted in 115 significantly overrepresented terms in SA and 96 in VA respectively (Supplemental File 3a and 3b (29)). Since the results showed significant overrepresentation at multiple levels within Reactome event hierarchy, we compared both adipocyte types at the root terms and subsequently focused on the most significantly enriched pathways relevant to the adipocytes or adipose tissue physiology/pathophysiology.

The overrepresentation analysis showed the most pronounced differences between both adipocyte types, where the upregulated proteins of SA are involved in wider spectra of cell processes in comparison to VA. SA are enriched especially with pathways and processes involved in extracellular matrix organization (FDR: 8.84E-04), vesicle-mediated transport (FDR: 7.44E-03), protein localization (FDR: 3.90E-02), or programmed cell death (FDR: 4.33E-02). Less

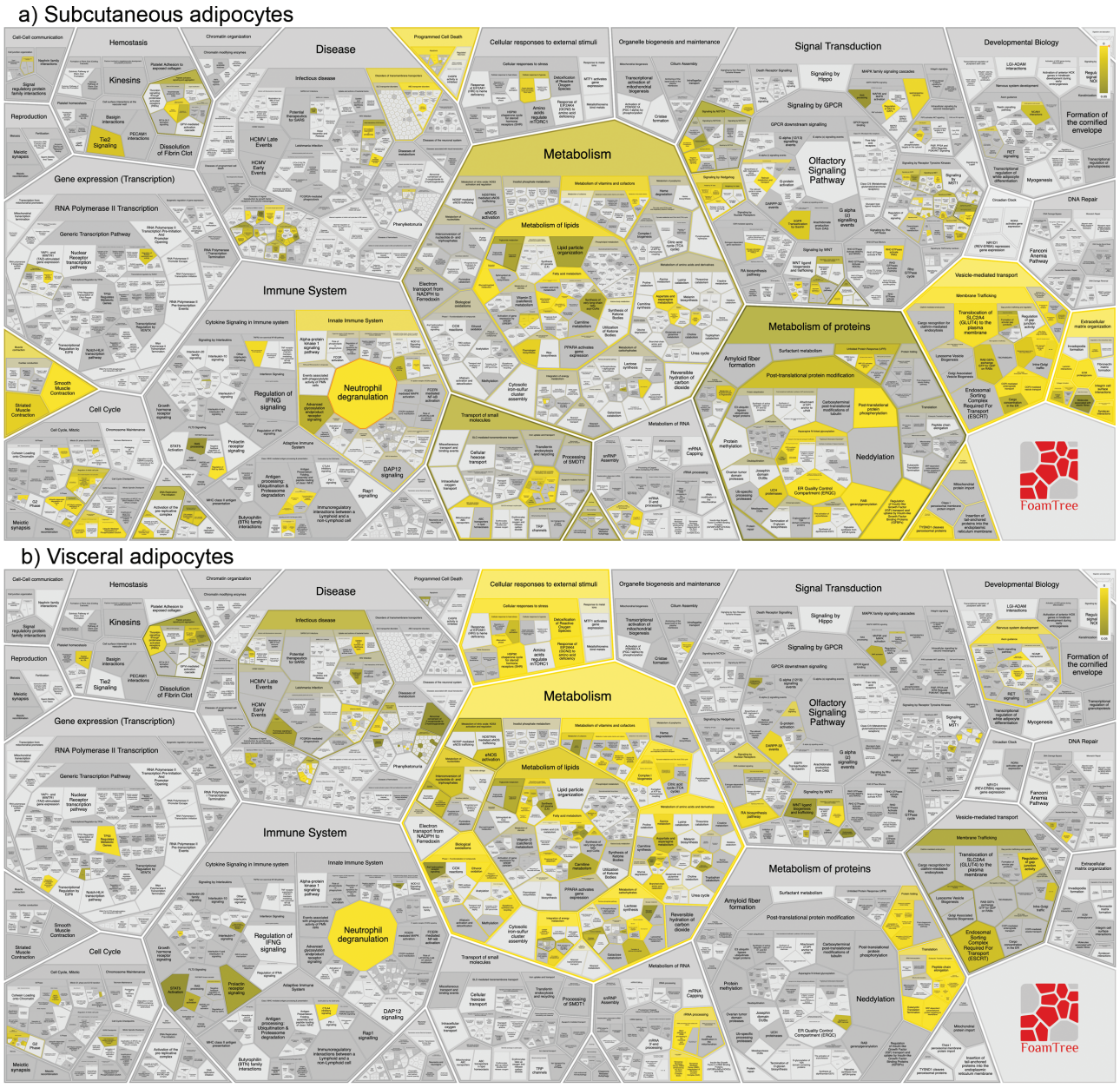

Figure 4. Pathway and reaction analysis of differentially expressed proteins. Reactome pathway and reactions enrichment analysis of all significantly a) SA and b) VA upregulated proteins. Figures show the most significant terms (P values < 0.05) using the Reactome build-in Voronoi diagram visualization tool. The terms are visualized based on the Reactome event hierarchy showing the most significant terms in bright yellow.

significant overrepresentation was also observed for processes and pathways in the metabolism (FDR: 1.08E-01), small molecule transport (FDR: 1.54E-01), and the protein metabolism (FDR: 1.72E-01) (Fig. 4A). In contrast to SA, upregulated proteins in VA are significantly overrepresented mainly in the metabolism (FDR: 3.56E-14) and cellular response to external stimuli (FDR: 3.10E-06) (Fig. 4B).

In order to select the most relevant Reactome pathways and reactions, both lists of significantly upregulated proteins were analyzed together in one analysis using Cytoscape ClueGO, showing only significant results and merging redundant groups with > 50% overlap (Supplemental file 4a (29)), but also separately for each adipocyte type (Supplemental file 4b and 4c (29)). Proteins often operate as a protein complex or interacting partners in complex networks. The identification of these protein networks and interactions is essential for understanding the functional properties of SA and VA proteins; however, not all interactions may have been recognized by the ontology enrichment analysis itself. Therefore, to extend the analysis of Reactome pathways and reactions, we also performed an interaction analysis using the STRING database scores. This created a large protein-protein interaction network combined with the most significantly enriched pathways

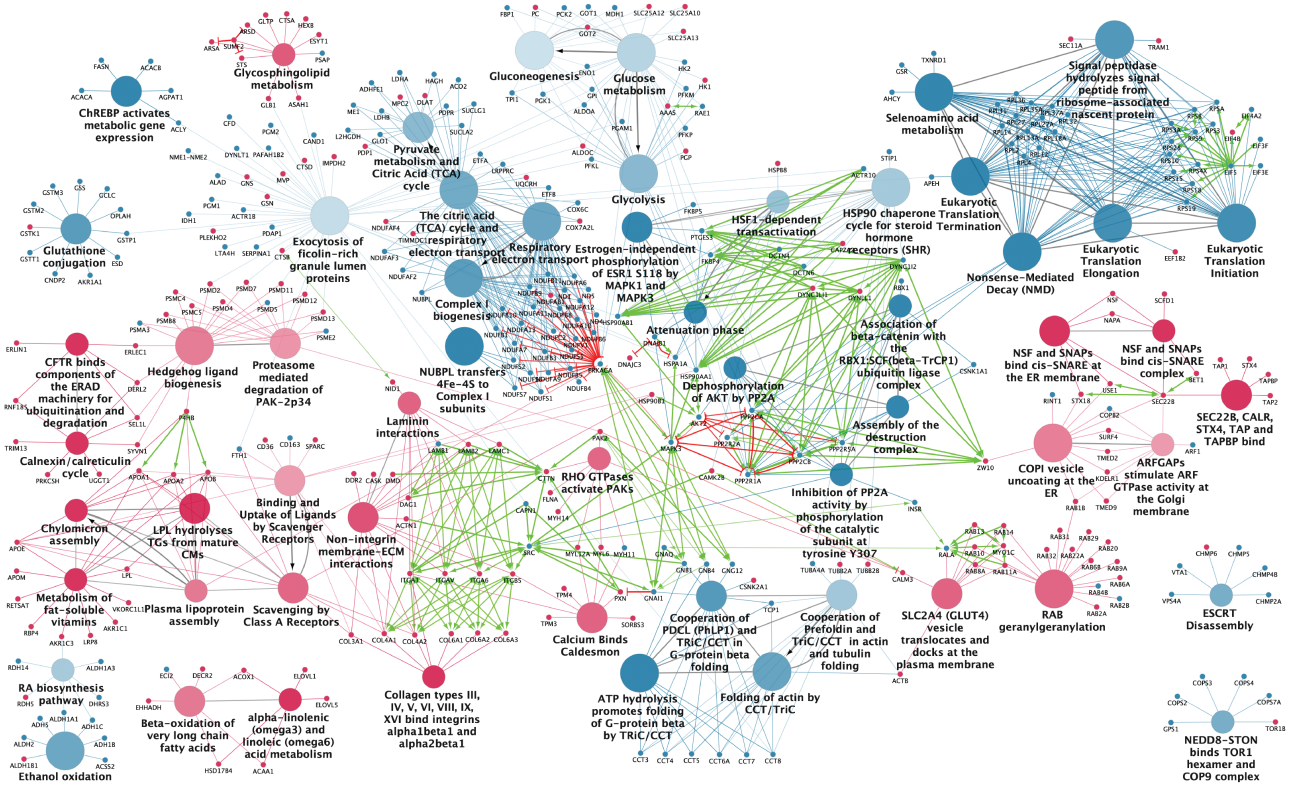

Figure 5. SA and VA upregulated proteins pathway and interaction analysis. The figure shows the most significant Reactome pathways and reactions (P values < 0.05) together with associated proteins and protein-protein STRING interaction links visualized using Cytoscape GlueGO+CluePedia plugin. SA and VA Reactome pathway and reaction term nodes are shown as red and blue circles, respectively. The size of the nodes indicates the significance of the node—the bigger, the more significant. Related terms connect edges of a gray color. Nodes sharing upregulated proteins of both groups are transparent. Bright red and green edges indicate the ability of the protein to activate or inhibit the coupled protein. The most significant terms of each cluster group were visualized and manually adjusted to obtain a reader-friendly pathway network. All pathways and networks with group cluster affiliation are accessible in Supplemental File 4 (29).

by the upregulated and downregulated proteins of SA, and vice versa for VA (Fig. 5). Some enriched groups of associated pathways, processes, and interactions share proteins of both groups; however, in order to simplify the complex network, we evaluated the pathways and processes separately for each adipocyte type.

SA pathways—vesicular transport and lipid metabolism

SA upregulated proteins enrichment analysis showed associations with chylomicron assembly and remodeling, together with other processes related to apolipoproteins, metabolism of fat-soluble vitamins, especially retinoid metabolism and transport, and ligand binding and uptake by scavenger receptors. Other metabolism-related processes include peroxisomal lipid metabolism with beta-oxidation of very-long-chain fatty acids. Another significantly enriched term was glycosphingolipid metabolism.

The enrichment of collagen proteins with several integrins and laminins implies extracellular matrix (ECM) interactions. Furthermore, the integrins were linked to proteins involved in caldesmon calcium binding process, which was also enriched by upregulated tropomyosin responsible for the regulation of glucose uptake. Furthermore, we observed proteins associated with proteasome mediated degradation, Hedgehog (Hh) ligand biogenesis and endoplasmic reticulum-associated degradation (ERAD). One of the largest SA upregulated protein clusters was formed by proteins of RAS-like family of small GTPases and other proteins involved in vesicle-mediated transport. The most enriched processes by these proteins were RAB geranylgeranylation, and RAB8A, 10, 13, 14 exchange GDP for GTP, together with insulin regulated trafficking by glucose transporter type 4 (GLUT4) and vesicle translocation and docking at the plasma membrane. Other processes related to this group of proteins include COPI vesicle uncoating at the endoplasmic reticulum, dissociation of cis-SNARE at the endoplasmic reticulum by the NSF ATPase activity, or proteins involved in antigen peptide transport and other transport processes.

VA pathways—energy metabolism and protein synthesis activity

Among the VA pathways we observed protein clusters involved especially in the energy metabolism. The most

significant enrichment was observed in the case of the protein cluster forming mitochondrial complex I. The complex I was also linked to proteins of the pyruvate metabolism and citric acid cycle. The enrichment analysis also shows proteins of glucose metabolism, glycolysis or gluconeogenesis, and other energy metabolism-related terms. In the context of the significant enrichment of processes associated with mitochondrial metabolism, we also observed proteins associated with glutathione conjugation. One of the largest protein clusters displays VA upregulated proteins involved in ribosomal assembly, translation initiation, and translation. This process is also connected to the group of protein phosphatases, which are associated with a regulation of translational activity by nonsense-mediated decay. Along with the elevated expression of translational apparatus proteins, we observed clusters of proteins involved in protein folding, activation, and stabilization like chaperonins and heat shock proteins in ATP-dependent manner. Further analysis showed several upregulated signaling proteins in VA. The network is centered around MAPK3, which is linked to several other signaling proteins such as AKT2, SRC, STAT5A, STAT5B, GNAI1, GNB1, and GNB4. Correspondingly, this was accompanied by the upregulation of several phosphatases, plausibly regulating the kinases in a negative feedback loop.

The Most Differentially Expressed Proteins

The top 20 most upregulated proteins from SA and VA are shown in Table 2 and Fig. 6A. We also ranked all proteins by mean intensity values to reveal the position of the most differentially expressed proteins within the entire proteome. The most profound differences are observable within the least abundant proteins (Fig. 6B). However, the majority of the most differentially expressed proteins by Log_2FC—especially GLIPR2, and ASPN, but also EZR, ALOX15, OGN, GPD1L, SLC38A10, PELO, CORO2B, and ANXA8L2—are among the more abundantly expressed proteins, which might suggest a major physiological role in distinguishing between SA and VA. Additionally, we plotted the intensities of the top 20 most differentially expressed proteins by Log_2FC, distinguishing experimental and missing imputed values in individual samples (Fig. 6C). This revealed several proteins potentially expressed exclusively either in SA (ALPL, CLIC6, TLCD2) or in VA (AGPAT9, ANXA8L2, PPAD1).

Prediction of Putative Secreted Proteins

Adipose tissue is an important endocrine organ that secretes several signaling molecules such as adipokines, which may contribute to the pathogenesis of obesity comorbidities. We submitted FASTA protein sequences of significant proteins with $Log_2FC > 1$ to the SignalP-5.0 Server. This server enables the prediction of the presence of secretory signal peptides transported by the Sec translocon and cleaved by Signal Peptidase I using deep neural networks (40). This analysis predicted 46 secreted proteins out of 175 SA upregulated proteins but only 20 among the 167 upregulated proteins in VA (Supplemental File 5 (29)). The 20 most differentially expressed SA proteins included 7 potentially secreted proteins that could therefore be possibly detectable in peripheral blood, namely ALPL, NOTCH3, FKBP9, GLB1, SIL1, RCN3, CD248. Similar to SA, we identified 6 proteins out of the 20 most upregulated proteins in VA with a prediction to be secreted, namely, OGN, ASPN, LUM, APCS, PRELP, and BGN.

We also performed an overrepresentation analysis of a predicted secreted proteins combined list using a combination of STRING together with Reactome database enrichment, and ClueGO biological processes enrichment analysis. This analysis revealed several interacting protein groups mainly among SA proteins. The largest enriched group involved in chylomicron assembly, triglyceride-rich lipoprotein particle remodeling, cholesterol transfer activity, regulation of cytokine production in immune response, and other related processes contained upregulated SA proteins APOA1, APOA2, APOB, APOE, ADAM10, CLU, DAG1, RCN, and TINAGL1 and the upregulated VA protein APOA4. A significant association was also observed for SA upregulated NENF and NUCB2, which were associated with negative appetite regulation. Additional significantly enriched terms worth mentioning included dermatan sulfate (VA: BGN, DCN) and keratan sulfate biosynthetic process (SA: GNS, GLB1; VA: LUM, OGN, PRELP).

Association of Clinical Traits With the Protein Expression

To investigate the association of clinical traits with the SA and VA proteome signatures, we adapted the WGCNA package in R which facilitates the identification of highly similar expression patterns and the subsequent correlation of these patterns with clinical data. Using the WGCNA co-expression network analysis, we obtained 11 and 16 modules of highly correlated proteins for SA and VA respectively (Supplemental File 6 (29)). The modules were assigned colors independently for the SA and VA proteomes. The analysis of VA also contained a grey module of proteins which were not assigned to any module. The module eigengenes (ME) were then correlated with the clinical data to identify modules with significant associations for SA (Fig. 7) and VA (Fig. 8) respectively. The functional enrichment of significantly correlated modules was performed

Table 2. Top 20 most upregulated proteins of SA and VA

	UniProt ID	Protein name	Gene name	Log_2FC	adj. *P* value
Subcutaneous adipocytes	**P05186**	**Alkaline phosphatase, tissue-nonspecific isozyme**	**ALPL**	**5.30**	**2.81E-13**
	Q9HBR0	Putative sodium-coupled neutral amino acid transporter 10	SLC38A10	4.08	3.97E-16
	Q5T5P2	Sickle tail protein homolog	KIAA1217	4.04	2.47E-09
	Q9H4G4	Golgi-associated plant pathogenesis-related protein 1	GLIPR2	3.97	4.76E-13
	Q96NY7	Chloride intracellular channel protein 6	CLIC6	3.72	3.78E-13
	Q14558	Phosphoribosyl pyrophosphate synthase-associated protein 1	PRPSAP1	3.48	1.21E-08
	A6NGC4	TLC domain-containing protein 2	TLCD2	3.44	8.14E-15
	Q9UM47	**Neurogenic locus notch homolog protein 3**	**NOTCH3**	**3.29**	**9.14E-14**
	Q9UQ03	Coronin-2B	CORO2B	3.16	1.80E-12
	Q9BRX2	Protein pelota homolog	PELO	3.03	3.39E-03
	O95302	**Peptidyl-prolyl cis-trans isomerase FKBP9**	**FKBP9**	**3.00**	**7.93E-12**
	Q9NR28	Diablo homolog, mitochondrial	DIABLO	2.95	2.77E-04
	P08473	Neprilysin	MME	2.93	7.14E-08
	P16278	**Beta-galactosidase**	**GLB1**	**2.89**	**9.13E-11**
	P22413	Ectonucleotide pyrophosphatase/phosphodiesterase family member 1	ENPP1	2.83	2.59E-07
	Q9H173	**Nucleotide exchange factor SIL1**	**SIL1**	**2.80**	**3.35E-05**
	P21926	CD9 antigen	CD9	2.76	1.41E-11
	Q96D15	**Reticulocalbin-3**	**RCN3**	**2.75**	**2.47E-09**
	Q9Y4F1	FERM, RhoGEF, and pleckstrin domain-containing protein 1	FARP1	2.71	6.91E-10
	Q9HCU0	**Endosialin**	**CD248**	**2.50**	**1.57E-12**
Visceral adipocytes	P02786	Transferrin receptor protein 1	TFRC	-2.39	6.09E-05
	Q8N6C5	Immunoglobulin superfamily member 1	IGSF1	-2.45	4.60E-06
	O75891	Cytosolic 10-formyltetrahydrofolate dehydrogenase	ALDH1L1	-2.46	2.54E-12
	O95671	N-acetylserotonin O-methyltransferase-like protein	ASMTL	-2.48	1.60E-04
	P27487	Dipeptidyl peptidase 4	DPP4	-2.58	3.41E-05
	P21810	**Biglycan**	**BGN**	**-2.61**	**3.15E-05**
	P51888	**Prolargin**	**PRELP**	**-2.64**	**4.22E-04**
	O95433	Activator of 90 kDa heat shock protein ATPase homolog 1	AHSA1	-2.74	3.39E-03
	P02743	**Serum amyloid P-component**	**APCS**	**-2.84**	**3.10E-09**
	P51884	**Lumican**	**LUM**	**-2.93**	**1.83E-04**
	Q9BXN1	**Asporin**	**ASPN**	**-3.03**	**9.39E-08**
	Q8N335	Glycerol-3-phosphate dehydrogenase 1-like protein	GPD1L	-3.05	1.53E-08
	P20962	Parathymosin	PTMS	-3.12	3.39E-05
	P15311	Ezrin	EZR	-3.13	6.70E-07
	P49915	GMP synthase [glutamine-hydrolyzing]	GMPS	-3.21	9.14E-14
	P16050	Arachidonate 15-lipoxygenase	ALOX15	-3.30	2.20E-09
	Q53EU6	Glycerol-3-phosphate acyltransferase 3	AGPAT9	-3.50	9.14E-14
	P20774	**Mimecan**	**OGN**	**-3.57**	**6.25E-06**
	Q5VT79	Annexin A8-like protein 2	ANXA8L2	-3.81	7.41E-12
	Q13442	28 kDa heat- and acid-stable phosphoprotein	PDAP1	-4.00	3.80E-08

The table provides a list of the 20 most differentially expressed proteins for SA and VA, respectively. Fold-change and significance of changes of the LIMMA differential expression analysis are demonstrated as log_2 fold-change (Log_2FC) and adjusted *P* value for multiple hypothesis testing. Potentially secreted proteins are in bold.

using the STRING database and GS was used to measure the degree of association between the traits and individual proteins (SA, Supplemental File 7; VA, Supplemental File 8 (29)).

SA module-trait correlation analysis showed that several modules were significantly associated with the clinical traits (Fig. 7). A positive correlation of waist circumference measured at the inferior margin of the ribs (waist1) was observed for the SA Purple and Salmon module, and a negative correlation was associated with the Red module. The SA Purple module (n = 76) eigengenes also correlated with the hip circumference, BMI, and DXA lean mass index. Although the Purple module was enriched by proteins involved in immune response and proteins associated with a response to infectious disease, the subsets of proteins significantly associated with the traits were enriched mainly

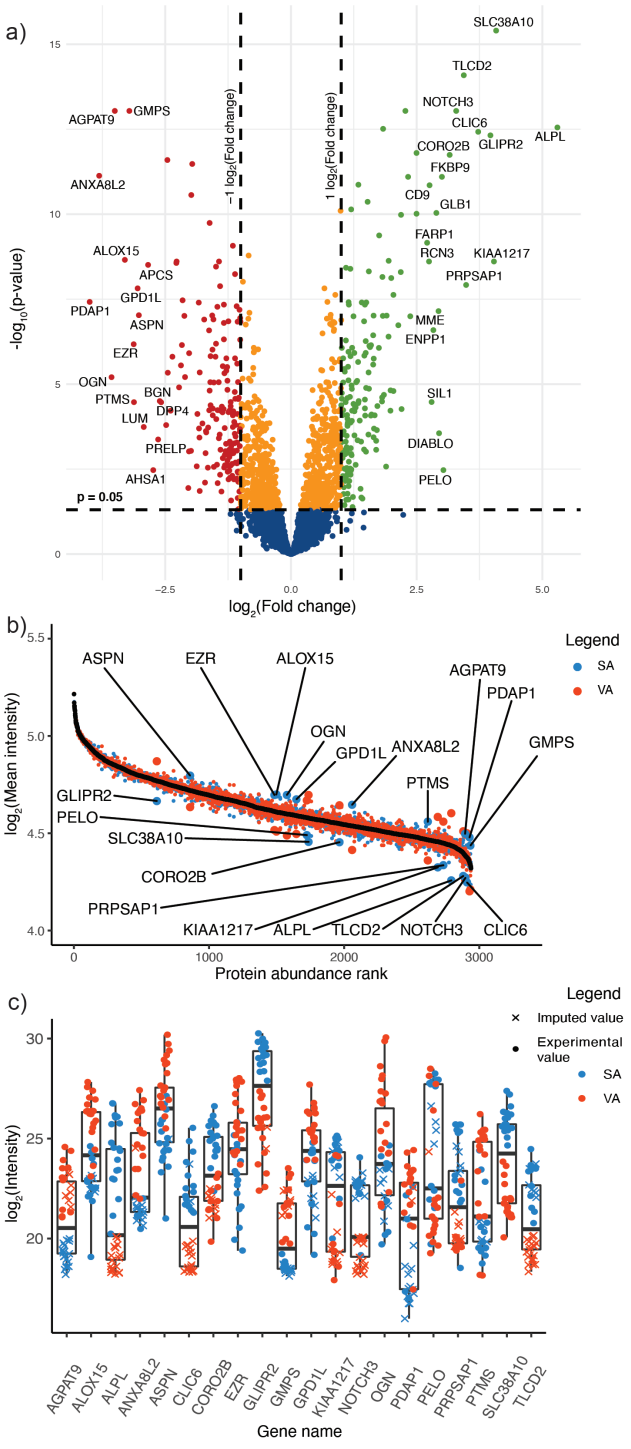

Figure 6. The most differentially expressed proteins. a) Volcano plot for differential protein expression analysis showing the top 20 most upregulated proteins of SA (green) and VA (red). b) Protein abundance rank of the most differentially expressed proteins. The mean intensity values of all measured proteins were ordered from the larger to the lowest values and ranked accordingly. The plot shows the relative representation of the most differentially expressed proteins within the whole adipocyte proteome. c) The box plot shows the differences between SA and VA intensity values of the most differentially expressed proteins. Cross stands for imputed values and dot for experimental intensity values.

by proteins of extracellular space and extracellular matrix disassembly, eg, CD44, CTSL, LCP1, or CAPN2. The SA Salmon module (n = 38) enriched by proteins in the RNA binding process was also positively correlated to the DXA visceral fat mass. The Red module (n = 200) associated with the negative correlation was enriched by proteins involved in vesicle-mediated transport and in the transport of small molecules, along with G protein signaling pathways. In addition to the Purple module, hip circumference and DXA lean mass index also correlated with the SA Green-yellow module (n = 75) enriched by proteins involved in the RNA metabolism, and the SA Black module (n = 177) enriched by proteins involved in immune system processes and stress response. The SA Black module was also associated with a positive correlation with HDL levels. A negative correlation with HDL levels and conversely a positive correlation with glycemia was linked to the SA Turquoise module (n = 719) enriched by proteins involved in vesicular transport and the protein metabolism. The subsets of significantly associated proteins with HDL levels and glycemia were associated especially with proteins involved in proteasomal protein catabolic process and regulation of G2/M transition of the mitotic cell cycle. Likewise, a positive correlation to glycemia and cholesterol levels was observed for the SA Brown module (n = 406) enriched by proteins involved in the translation and metabolism of proteins. Conversely, a negative correlation was observed with the SA Green module (n = 541) enriched significantly by mitochondrial proteins and proteins involved in the citric acid and respiratory electron transport. The most significant positive correlation of SA proteins with glycemia was observed for FAM129B (GS = 0.82), PIN1 (GS = 0.81). Conversely, the most significant negative correlation was observed for PXN (GS = 0.80), or HIBADH (GS = −0.80) accompanied by other dehydrogenases, eg, ACAD11 (GS = −0.79), ACADM (GS = −0.74), or HSDL2 (GS = −0.74) involved in fatty acid beta-oxidation. An inverse correlation to cholesterol level was observed for the SA Blue module (n = 433), enriched by proteins of the endomembrane system, especially proteins of the endoplasmic reticulum, and the Pink module (n = 163) enriched by ribosomal proteins and proteins involved in intracellular transport and localization. The overall most significant correlation to cholesterol was associated with the RAB22A (GS = −0.84), LGALS12 (GS = −0.78) and STX-8 (GS = −0.74).

The VA module-trait correlation analysis (Fig. 8) showed different correlation patterns compared to the SA proteome. A positive correlation with waist measured at the umbilical level and total body fat was associated with the VA Green-yellow module (n = 124) enriched by organelle organization and translational initiation. A negative

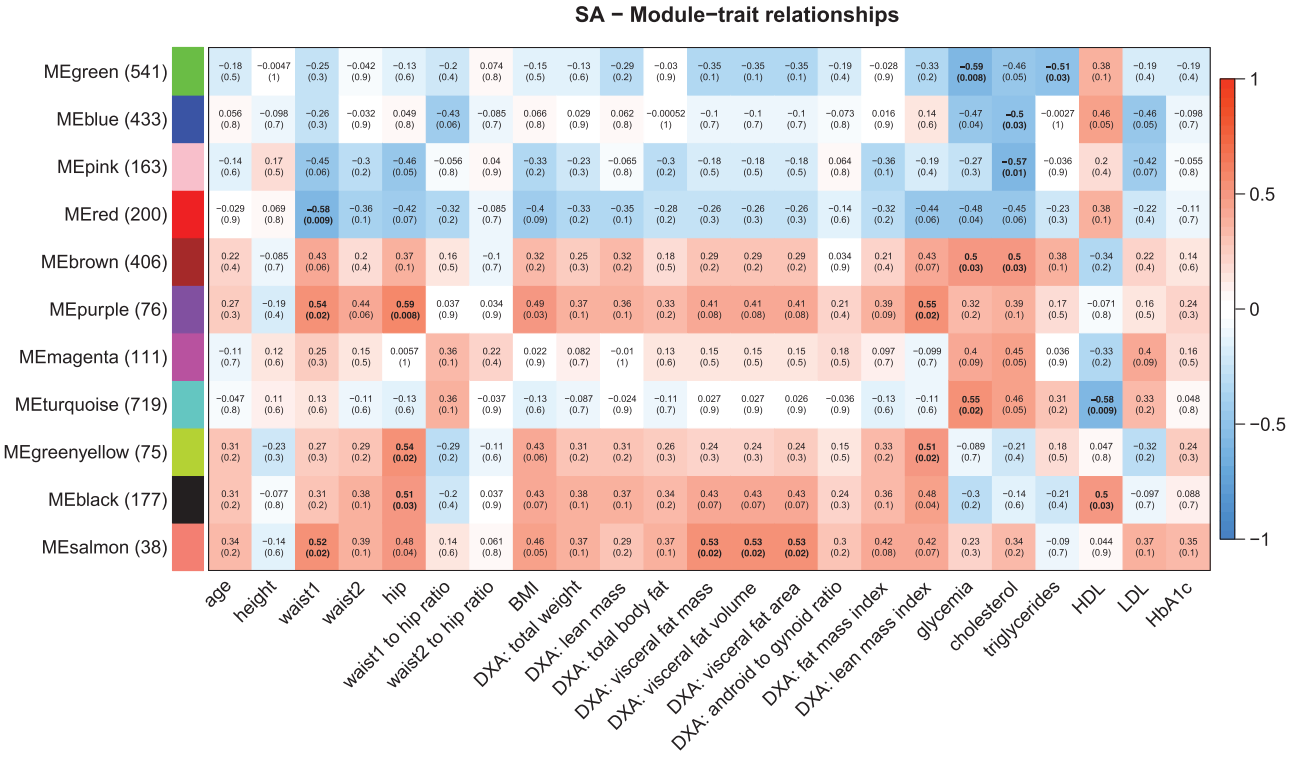

Figure 7. SA module-trait relationships. SA module-trait relationship and corresponding *P* values (Pearson) between the module eigengenes and selected clinical traits. Strong positive correlations are in red, while strong negative correlations are blue, numbers in individual cells are correlation coefficient (*P* value). Significant module-trait correlations ($P < 0.05$) with the absolute correlation value >0.5 are in bold. The size of the modules is in brackets. Waist1 stands for the waist circumference measured at the inferior margin of the ribs, and waist2 measured at the umbilical level.

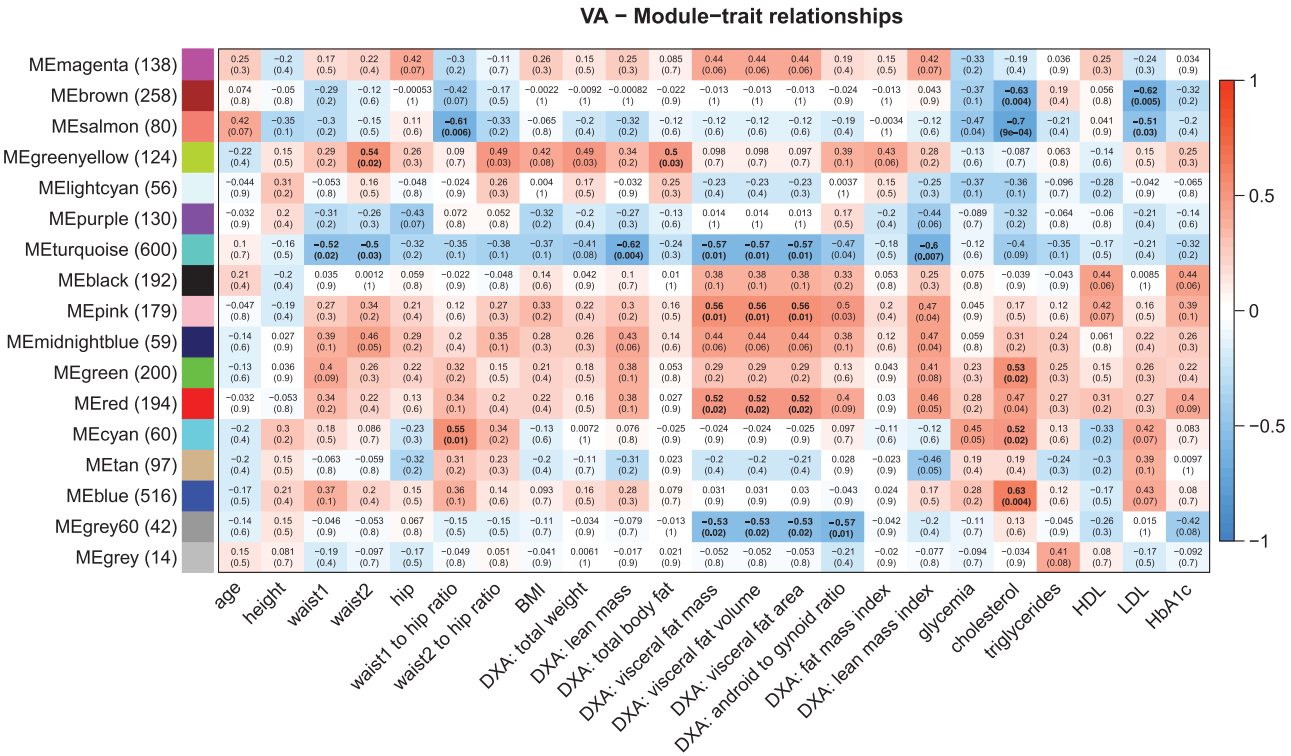

Figure 8. VA module-trait relationships. VA module-trait relationship and corresponding *P* values (Pearson) between the module eigengenes and selected clinical traits. Strong positive correlations are in red, while strong negative correlations are blue, numbers in individual cells are correlation coefficient (*P* value). Significant module-trait correlations ($P < 0.05$) with the absolute correlation value > 0.5 are in bold. The size of the modules is in brackets. Waist1 stands for the waist circumference measured at the inferior margin of the ribs, and waist2 measured at the umbilical level.

correlation with both waist circumferences, but also with DXA lean mass and DXA visceral fat mass, was associated with the VA Turquoise module (n = 600). The VA Turquoise module is enriched largely by processes in mitochondria, such as the citric acid cycle and respiratory electron transport or fatty acid metabolism. The most significant association with the DXA visceral fat mass was observed for NADH dehydrogenases, especially NDUFB8 (GS = –0.82) and NDUFB4 (GS = –0.79). A negative correlation with the DXA visceral fat parameters was also observed for the VA Grey60 (n = 42) module that is enriched by proteins in carboxylic acid and small molecule metabolic processes. Conversely, a positive correlation was associated with the VA Pink (n = 159) and Red module (n = 194). The VA Pink module is enriched by proteins in actin cytoskeleton organization and metabolism of RNA, whereas the VA Red module is enriched by proteins involved in vesicle-mediated transport and exocytosis. A positive correlation was also observed for cholesterol and the VA Blue, Green, and Cyan modules. The VA Blue module (n = 516) is enriched by proteins involved in the cellular metabolic processes, whereas, the VA Green module (n = 200) is enriched by proteins involved in antigen processing and the presentation of peptide antigens, and proteasome degradation. The VA Cyan module (n = 60), which is also associated with the waist1 to hip ratio, is enriched by cytosolic proteins. Similar to the Cyan module but with a negative correlation, the VA Salmon module (n = 80) enriched by proteins in oxidative phosphorylation was associated with cholesterol but also with LDL levels. Here, the most significant association with cholesterol was observed for RAB43 (GS = –0.82) and ECHDC3 (GS = –0.81). Also, a negative correlation to cholesterol and LDL levels was observed for the VA Brown module (n = 258). This module is significantly enriched by proteins involved in the vesicle-mediated transport and lipid metabolism. The most significant negative correlation with cholesterol (GS = –0.81) and LDL (GS = –0.82) was observed for ANTXR2.

Discussion

In our study, we focused on the comparison of protein expression profiles from mature adipocytes isolated from abdominal SAT and omental VAT collected from severely obese women in order to explore major depot-specific differences. We identified 3686 proteins groups and found 1140 differentially expressed proteins (adj. *P* value < 0.05), of which 576 proteins were upregulated in SA and 564 in VA samples. Our analysis revealed cell-specific protein expression patterns of coordinated processes in both adipocyte proteomes. Most of the protein clusters observed in the global correlation mapping contained functionally or mechanistically related protein clusters also observed in the enrichment analysis of differentially expressed proteins. Our study demonstrated that SA are more active in processes related to vesicular transport and secretion, together with increased lipid metabolism activity. Conversely, the expression of proteins involved in translational or biosynthetic activity and energetic metabolism was higher in VA. Moreover, the functional differences were further highlighted by distinct correlations with the clinical and body composition data.

Oxidative phosphorylation is essential in the metabolism by supplying ATP for cellular processes. Our results indicate that oxidative phosphorylation, and processes related to mitochondria and the mitochondria energy metabolism, represent one of the most pronounced differences between SA and VA. The global correlation cluster mapping of the VA proteome showed more balanced and significantly higher correlations of the mitochondrial proteins and proteins involved in mitochondrial processes in comparison to SA. The pathway analysis of differentially expressed proteins then indicated that especially the proteins of mitochondrial electron transport chain complex I, pyruvate metabolism, and citric acid cycle are more abundantly expressed in VA. Our results are in agreement with several lines of evidence indicating that the visceral compartment is generally characterized by a relatively higher mitochondrial oxidative metabolism (41, 42). This could be further underlined by obesity-induced changes that differentially affect mitochondria in SA and VA. More specifically, previous studies showed a negative correlation between oxidative phosphorylation capacity and BMI, and between electron transfer system capacity and BMI in SA but not in VA (43, 44). Since our analysis investigated the proteome of adipocytes derived from the extreme phenotype of body composition, we can hypothesize that observed differences might to some extent serve as an indicator of SA mitochondria impairment, which could in turn contribute to the enhanced energetic and metabolic activity of VA. Further, underlining the relevance of bioenergetics metabolism, the number of proteins involved in mitochondrial regulation showed significant negative correlation with clinical and body composition parameters including glycemia, triglycerides level, waist to hip ratio, LDL, and cholesterol. Notably, the systematic downregulation of oxidative phosphorylation (OXPHOS) capacity and mitochondrial reorganization as a general alteration of adipocytes in obesity was also recently reported in the diet-induced obesity murine model, affecting both depots, with larger changes observed in SA (45).

In addition to OXPHOS, anaerobic glycolysis also contributes to ATP synthesis; previous findings suggest that in adipocytes it is in fact a more relevant energy source

in adipocytes (46). In this study, we observed a group of proteins involved in glycolysis to be more abundantly expressed in VA (eg, ALDOA, ENO1, GPI, HK2, PFKL, PFKM, PFKP, PGAM1, PGK1, PPP2CA), which might reflect the overall higher energy demand of VA, as well as a partial compensatory mechanism for overloaded mitochondria. This is also in agreement with previous findings that the OXPHOS capacity of VA adipocytes remained unaffected with higher BMI, while glycolysis increased (44). The upregulated expression of glycolytic pathway proteins might also be the consequence of inferior capillary density and limited angiogenic growth capacity of visceral tissue, potentially leading to local hypoxia and a shift towards an anaerobic metabolism in less vascularized areas (47). Notably the glycolytic pathway yields intermediates that are further utilized in aerobic cellular bioenergetics, which also appeared to be upregulated in VA in our study. This includes enzymes directly involved in the TCA and pyruvate metabolism (eg, ACO2, ADHFE1, GLO1, HAGH, L2HGDH, LDHA, LDHB, ME1, PDPR, SUCLA2, SUCLG1), as well as in the above-mentioned upregulation of several complex I proteins. Furthermore, in VA we revealed a higher abundance of ATP-citrate lyase (ACLY), the enzyme responsible for the cytosolic synthesis of acetyl-CoA from citrate, and higher protein expression of other lipogenic enzymes including ACACA, ACACB, FASN, and HACD3. Altogether, our results support the notion that glycolytic and lipogenic processes are augmented in VA. This is further clarified by the fact that several enzymes involved in the regulation of these processes are among the most expressed proteins of VA (eg, AGPAT9, GPD1L). This is in agreement with previous reports of increased glucose uptake rates in VA, particularly in obese individuals, where VAT acts as an essential glucose sink (48).

Metabolic activity requires newly synthesized proteins to be complemented by molecular chaperones which assist their folding into native three-dimensional states. This process should be further accompanied by intracellular trafficking in order to deliver the synthesized proteins into different organelles. The potential demand for novel proteins in the VA is supported by the overexpression of protein groups including multiple chaperones, ribosomal proteins and elongation factors, and dynactin complex subunits. This correlates with previous studies reporting the superior upregulation of genes involved in protein synthesis in the visceral compartment (42). Moreover, the increase of several members of the COP9 (Constitutive photomorphogenesis 9) signalosome involved in the regulation of ubiquitin-proteasome pathway, along with the ESCRT (endosomal sorting complexes required for transport) complex, also argues for tightly orchestrated proteostasis in VA. In comparison, in SA we observed an overrepresentation of components of 26S proteasome machinery (eg, PSMB8, PSMC4, PSMC5, PSMD11, PSMD12, PSMD13, PSMD2, PSMD4, PSMD7), and proteins involved in the endoplasmic reticulum-associated degradation (ERAD) pathway (eg, DERL2, ERLEC1, ERLIN1, RNF185, SEL1). Further, we revealed the upregulation of the Calnexin/Calreticulin chaperone system dedicated to N-glycosylated proteins folding, which, in line with previous studies, also suggests enhanced protein traffic along the secretory pathway in SA (49, 50). This is also well illustrated by the upregulation of SIL1 and RCN3, involved in secretory trafficking, which are among the most overexpressed SA proteins. This system plays a vital role in Ca^{2+} homeostasis and ensures that assembled glycoproteins leave the endoplasmic reticulum, or orchestrate their degradation via ERAD, when correct protein folding is unachievable (51). Importantly, the expression of several members of this pathway is elevated as a result of ER stress and is a part of unfolded protein response. For instance, UGGT—significantly overrepresented in SA in our study—plays the role of a checkpoint allowing misfolded proteins to rebind to the chaperones, thus preventing their exit from the ER (51).

This study also clarifies depot-specific differences between numerous modes of vesicular trafficking systems. Trafficking between subcellular compartments involves transport containers whose formation is orchestrated by multiple conserved coat complexes. These encompass the coat protein complexes (COPI and II) involved in endoplasmic reticulum export and clathrin and caveolin coat families involved in the subsequent steps defined by the exocytic and endocytic pathways (52). Additionally, cargo capture is necessarily connected to cellular components that direct the transport of vesicles to their unique destinations. Two large protein families that contribute significantly to vesicle targeting are the Rab GTPases and the soluble N-ethyl-maleimide-sensitive factor attachment protein receptor (SNARE) family of docking/fusion proteins (52). In our study, upregulation in the above-mentioned trafficking networks was observed in SA, reflecting either increased intracellular transport of various cargo or the extensive regulation of lipid droplet formation and interactions with other organelles, such as endosomes, peroxisomes, and mitochondria, where lipids and signaling molecules are exchanged (53). Remarkably, this is well in line with our data that showed the enrichment of predicted secreted proteins in SA, compared with VA. It is also noteworthy to underline the enrichment of RABs which are also involved in the transport pathway, including the trafficking of high-affinity glucose transporter GLUT4 (54). In agreement with our results, multiple proteins involved in vesicular trafficking were previously reported by Xie and colleagues, who characterized the SA proteome in lean men (50). Highlighting

the variability in transport mechanisms, it is also worth noting that the number of VA proteins associated with the vesicle-mediated transport is negatively correlated with cholesterol and LDL levels, and positively with visceral fat mass. In addition, the largest SA module (Turquoise) is enriched in proteins involved in vesicular transport and positively correlated to glycemia and negatively to HDL level. Altogether, our data suggest distinct features of protein synthesis, transport, and turnover in adipocytes from different depots.

In adipocytes, triglycerides (TG) are synthesized from free fatty acids (FFAs) esterified to a glyceride-glycerol backbone. The majority of FFAs are delivered through lipoprotein lipase (LPL) breakdown of triglyceride-rich plasma lipoproteins. This process is partially complemented by the direct uptake of circulating FFA (5). In the current study, we observed the overexpression of several lipid homeostasis regulators in SA, encompassing the main gatekeeper enzyme for the entry and FFA re-esterification in adipose tissue—LPL, crucial long-chain fatty acid transporter in adipocytes CD36, and proteins of the apolipoprotein family (eg, APOA1, APOA2, APOB, APOD, APOL2, APOM, and APOE). Notably, the expression of hormone-sensitive lipase (LIPE), the rate-limiting step for lipolysis of triglycerides stored in adipocytes, was higher in VA. Apolipoproteins regulate the assembly of lipoprotein particles, maintain their structure, and affect their metabolism by binding to membrane receptors (55). In agreement with our results, higher mRNA expression of APOE was previously reported in SA (56). Conversely, another study revealed a higher level of APOA1 and APOE in a visceral depot in a mixed-sex cohort (42). Nonetheless, further research is needed, as this is—to the best of our knowledge—the first proteomic study to unveil such pronounced depot-specific differences in multiple apolipoproteins in mature adipocytes. In addition to LPL-catalyzed hydrolysis of triglycerides, it is worth mentioning that lipoproteins may also be whole-particle internalized directly by cells through LDL receptor family member proteins such as VLDLR, LDLR, and LRP1 (57), which were, in comparison, upregulated in VA. Notably, several other lipid metabolism regulators were overexpressed in SA, including ACOX1, a rate-limiting enzyme in peroxisomal fatty acid β-oxidation, and a cluster of proteins involved in the glycosphingolipid metabolism (eg, ARSA, ARSD, ASAH1, CTSA, ESYT1, GLB1, GLTP, HEXB, STS, SUMF2). This is of particular importance, as disturbances in glycosphingolipid content regulation emerged as an essential contributor to the development of insulin resistance (58). Altogether, our data imply large lipid flux and the prominent role of the lipoprotein metabolism in a subcutaneous compartment, suggesting distinct depot-dependent features of triglyceride utilization.

Obesity is characterized by considerable adipose tissue expansion, and ECM reorganization creates space for adipocyte enlargement. In line with this, proteins associated with cytoskeletal and ECM remodeling were in our study significantly correlated with increased visceral fat mass (VA, Pink module). ECM is a complex structure composed of different proteins, proteoglycans, and polysaccharides (59). In the current study, we revealed prominent upregulation in ECM components including collagens (eg, COL3A1, COL4A1, COL4A2, COL6A1, COL6A2, COL6A3), laminin (LAMB2, LAMC1), and integrin (eg, ITGA1, ITGA6, ITGAV, ITGB5) in SA. The importance of ECM remodeling in a distinctive pathological contribution of adipose tissue depending on its anatomical site was previously demonstrated by CILAIR-based comparative secretome analysis of obese VAT and SAT (60). Remarkably, we found that the majority of the VAT most oversecreted proteins mentioned in this study is in fact enriched in SA in our analysis (eg, COL6A3, LAMC1, HSPG2, CD14). By contrast, 2 of the most oversecreted SAT proteins (COL1A2, THBS1) identified by Roca-Rivada et al (60) were found enriched in VA in our study. This negative correlation might suggest protein depletion in cellular fraction due to high secretory activity. Nonetheless, these discrepancies might also be attributed to dissimilar experimental set-up, including differences in cohorts, methodology, and analysis of whole tissue vs isolated mature cells. Further, the SA expression of proteins involved in extracellular matrix disassembly, ie, CD44, CTSL, LCP1, or CAPN2, correlated with the clinical data including waist to hip ratios, total weight, or BMI. Significantly, several studies implicate a causal role of CD44 in adipose tissue inflammation and insulin resistance (61, 62). In a similar manner, another emerging regulator of ECM interactions involved in insulin resistance, CD248, is among the most expressed proteins of SA (63).

In our study, 5 of the most upregulated proteins of VA were small leucine-rich repeat proteoglycans (SLRPs), ubiquitous ECM components involved in matrix structural organization (OGN, ASPN, LUM, PRELP, and BGN). Indeed, SLRPs have previously been reported in insulin resistance-associated visceral secretome, show a positive correlation with BMI and central obesity, and play overall substantial roles in mediating metabolic inflammation (64-66). Together, these proteins may be considered to constitute promising targets for following research of the depot-specific imprint in the peripheral system. Altogether, ECM components emerge as an additional essential player in the pathophysiology of obesity, and it is plausible that the depot-specific composition of ECM and its interactions are directly implicated in the processes associated with adipose tissue dysfunction.

To conclude, our study characterized the proteome of mature adipocytes from subcutaneous and visceral adipose depots. Of special interest are proteins that are predicted or annotated as secretory and could be utilized as promising depot-specific biomarkers for advanced obesity monitoring. Previously published data concerning obesity emphasize the activity and deleterious role of the visceral compartment. In addition to this widely accepted concept, our results highlight the role of subcutaneous adipocytes in the regulation of fundamental processes associated with obesity, including the lipid metabolism, vesicular transport, and ECM composition.

This is to date the most comprehensive comparative proteomic analysis of isolated adipocytes; however, some limitations must be considered. Our study focused on female patients with clinically severe obesity, as they represent the primary group of bariatric surgery patients (67). Extrapolations of our data should thus be approached with caution; the differences reported here must be confirmed in future mixed cohort studies employing a combination of functional and metabolomics approaches. Furthermore, while the extreme phenotype of our cohort is useful in the enhancement of differences between studied depots, any extrapolation of our results to nonobese subjects remains questionable, as well as any inference of causality based on observed data. On the other hand, to the best of our knowledge this is the first large-scale non-targeted proteomics analysis of abdominal SA and omental VA derived from paired biopsies of a relatively homogenous and large (n = 19) cohort, performed together with a bioinformatic analysis of the whole proteome, and differentially expressed proteins. Our effort provides insight into the functional role of adipocytes in obesity and may thus serve as a roadmap for future research. A better understanding of the distinct roles of adipocytes will help improve the characterization of the molecular pathophysiology of obesity and its associated diseases and facilitate relevant therapeutic interventions.

Acknowledgments

The authors wish to acknowledge the contribution of Mgr. Jitka Machackova (data collection), Mgr. Hana Valentova (sample collection), Martin Bolek, MD (patient identification), and Mgr. David Konecny (proofreading).

Financial Support: This study was supported by a Specific University Research grant No. MUNI/A/1307/2019 and MUNI/A/1246/2020 provided by the Ministry of Education, Youth and Sports of the Czech Republic. D.K. was supported by the internal research grant MUNI/A/1615/2020. CETOCOEN PLUS project CZ.02.1.01/0.0/0.0/15_003/0000469 (CEP: EF15_003/0000469), RECETOX research infrastructure (Ministry of Education, Youth and Sports of the Czech Republic: LM2018121), CETOCOEN EXCELLENCE Teaming 2 project supported by Horizon2020 (857560) and the Ministry of Education, Youth and Sports of the Czech Republic (02.1.01/0.0/0.0/18_046/0015975). CIISB, Instruct-CZ Centre of Instruct-ERIC EU consortium, funded by MEYS CR infrastructure project LM2018127, is gratefully acknowledged for the financial support of the measurements at the CEITEC Proteomics Core Facility. Computational resources were supplied by the e-Infrastruktura CZ project (e-INFRA LM2018140) provided within the program Projects of Large Research, Development and Innovations Infrastructures.

Author Contributions: Conceptualization, P.Hr., J.K., and J.B.V.; Clinical assessment and sample biopsies, M.P., P.Ho., M.M., and M.B.; Cell handling, J.K., and P.L.; LC-MS, D.P., and Z.Z.; Data analysis, P.Hr., D.K., and D.P., Investigation, and data interpretation, P.Hr., J.K., and J.F.K.; Writing—original draft P.Hr., and J.K.; Writing—Review & Editing, P.Hr., J.K, M.P., P.Ho., M.M., M.B., D.K., P.L., J.F.K., D.P., Z.Z., and J.B.V.; Visualization, P.Hr., D.K., Project administration and funding acquisition, J.B.V.

Additional Information

Correspondence: Julie Dobrovolna (previously Bienertova-Vasku), Department of Pathological Physiology, Faculty of Medicine, Masaryk University, Kamenice 5, Building A18, Brno 625 00, Czech Republic. Email: julie.dobrovolna@recetox.muni.cz.

Disclosures: The authors declare that no conflict of interest exists.

Data Availability: The mass spectrometry proteomics data and the search results have been deposited to the ProteomeXchange Consortium via the PRIDE (26) partner repository with the dataset identifier PXD024734. Supplementary data is available at figshare.com (doi:10.6084/m9.figshare.14626341 (28)). The R scripts are available upon request.

References

1. Sethi JK, Vidal-Puig AJ. Thematic review series: adipocyte biology. Adipose tissue function and plasticity orchestrate nutritional adaptation. *J Lipid Res*. 2007;**48**(6):1253-1262.
2. Schoettl T, Fischer IP, Ussar S. Heterogeneity of adipose tissue in development and metabolic function. *J Exp Biol*. 2018;**221**(Suppl 1):jeb162958.
3. Tchkonia T, Thomou T, Zhu Y, et al. Mechanisms and metabolic implications of regional differences among fat depots. *Cell Metab*. 2013;**17**(5):644-656.
4. Kwok KH, Lam KS, Xu A. Heterogeneity of white adipose tissue: molecular basis and clinical implications. *Exp Mol Med*. 2016;**48**:e215.
5. Lee MJ, Wu Y, Fried SK. Adipose tissue heterogeneity: implication of depot differences in adipose tissue for obesity complications. *Mol Aspects Med*. 2013;**34**(1):1-11.
6. Tchernof A, Després JP. Pathophysiology of human visceral obesity: an update. *Physiol Rev*. 2013;**93**(1):359-404.
7. Brockman D, Chen X. Proteomics in the characterization of adipose dysfunction in obesity. *Adipocyte*. 2012;**1**(1):25-37.
8. Gómez-Serrano M, Camafeita E, García-Santos E, et al. Proteome-wide alterations on adipose tissue from obese patients as age-, diabetes- and gender-specific hallmarks. *Sci Rep*. 2016;**6**:1–19.

9. Haard PMMV, Herbrink P, Schweitzer DH. Differentiation of paired human subcutaneous and visceral adipose tissues by holistic proteome profiling using LC-MS/MS: a pilot study. *Int J Res Stud Biosci*. 2016;**4**(7):32-42.
10. Murri M, Insenser M, Bernal-Lopez MR, Perez-Martinez P, Escobar-Morreale HF, Tinahones FJ. Proteomic analysis of visceral adipose tissue in pre-obese patients with type 2 diabetes. *Mol Cell Endocrinol*. 2013;**376**(1-2):99-106.
11. Vogel MAA, Wang P, Bouwman FG, et al. A comparison between the abdominal and femoral adipose tissue proteome of overweight and obese women. *Sci Rep*. 2019;**9**(1):4202.
12. Alfadda AA, Benabdelkamel H, Masood A, et al. Proteomic analysis of mature adipocytes from obese patients in relation to aging. *Exp Gerontol*. 2013;**48**(11):1196-1203.
13. Benabdelkamel H, Masood A, Almidani GM, et al. Mature adipocyte proteome reveals differentially altered protein abundances between lean, overweight and morbidly obese human subjects. *Mol Cell Endocrinol*. 2015;**401**:142-154.
14. Doulamis IP, Konstantopoulos P, Tzani A, et al. Visceral white adipose tissue and serum proteomic alternations in metabolically healthy obese patients undergoing bariatric surgery. *Cytokine*. 2019;**115**:76-83.
15. Perez-Riverol Y, Csordas A, Bai J, et al. The PRIDE database and related tools and resources in 2019: improving support for quantification data. *Nucleic Acids Res*. 2019;**47**(D1): D442-D450.
16. Adamczyk P, Bužga M, Holéczy P, et al. Bone mineral density and body composition after laparoscopic sleeve gastrectomy in men: a short-term longitudinal study. *Int J Surg*. 2015;**23**(Pt A):101-107.
17. Adamczyk P, Bužga M, Holéczy P, et al. Body size, bone mineral density, and body composition in obese women after laparoscopic sleeve gastrectomy: a 1-year longitudinal study. *Horm Metab Res*. 2015;**47**(12):873-879.
18. Pluskiewicz W, Buzga M, Holeczy P, Smajstrla V, Adamczyk P. A comment on 'Changes in bone mineral density in women following 1-year gastric bypass surgery' published by Casagrande DS et al. *Obes Surg*. 2013;**23**(11):1885.
19. Bužga M, Holéczy P, Švagera Z, Švorc P, Zavadilová V. Effects of sleeve gastrectomy on parameters of lipid and glucose metabolism in obese women - 6 months after operation. *Wideochirur Inne Tech Maloinwazyjne* 2013;**8**(1):22-8.
20. Bužga M, Holéczy P, Švagera Z, Zonča P. Laparoscopic gastric plication and its effect on saccharide and lipid metabolism: a 12-month prospective study. *Wideochirur Inne Tech Maloinwazyjne* 2015;**10**(3):398-405.
21. Carswell KA, Lee MJ, Fried SK. Culture of isolated human adipocytes and isolated adipose tissue. *Methods Mol Biol*. 2012;**806**:203-214.
22. Gallagher SR. One-dimensional SDS gel electrophoresis of proteins. *Curr Protoc Mol Biol*. 2012;**97**(1):10.2A.1-10.2A.44.
23. Wiśniewski JR, Rakus D. Multi-enzyme digestion FASP and the 'Total Protein Approach'-based absolute quantification of the Escherichia coli proteome. *J Proteomics*. 2014;**109**:322-331.
24. Wiśniewski JR, Zougman A, Nagaraj N, Mann M. Universal sample preparation method for proteome analysis. *Nat Methods*. 2009;**6**(5):359-362.
25. Yeung YG, Nieves E, Angeletti RH, Stanley ER. Removal of detergents from protein digests for mass spectrometry analysis. *Anal Biochem*. 2008;**382**(2):135-137.
26. Stejskal K, Potěšil D, Zdráhal Z. Suppression of peptide sample losses in autosampler vials. *J Proteome Res*. 2013;**12**(6):3057-3062.
27. Cox J, Mann M. MaxQuant enables high peptide identification rates, individualized p.p.b.-range mass accuracies and proteome-wide protein quantification. *Nat Biotechnol*. 2008;**26**(12):1367-1372.
28. R Development Core Team. *R: A Language and Environment for Statistical Computing*. R Foundation for Statistical Computing; 2016.
29. Hruska P, Kucera J, Pekar M, et al. Proteomic signatures of human visceral and subcutaneous adipocytes—supplementary files. Dataset posted on October 27, 2021. doi:10.6084/m9.figshare.14626341.v1.
30. Ritchie ME, Phipson B, Wu D, et al. limma powers differential expression analyses for RNA-sequencing and microarray studies. *Nucleic Acids Res*. 2015;**43**(7):e47.
31. Smyth GK, Michaud J, Scott HS. Use of within-array replicate spots for assessing differential expression in microarray experiments. *Bioinformatics*. 2005;**21**(9):2067-2075.
32. Benjamini Y, Hochberg Y. Controlling the false discovery rate: a practical and powerful approach to multiple testing. *J R Stat Soc Series B (Methodol)*. 1995;**57**(1):289-300.
33. Ward JH Jr. Hierarchical grouping to optimize an objective function. *J Am Stat Assoc* 1963;**58**(301):236-244.
34. Langfelder P, Horvath S. WGCNA: an R package for weighted correlation network analysis. *BMC Bioinformatics*. 2008;**9**:559.
35. Langfelder P, Horvath S. Fast R functions for robust correlations and hierarchical clustering. *J Stat Softw*. 2012;**46**(1):1-17.
36. Horvath S, Dong J. Geometric interpretation of gene coexpression network analysis. *PLoS Comput Biol*. 2008;**4**(8):e1000117.
37. Szklarczyk D, Gable AL, Lyon D, et al. STRING v11: protein-protein association networks with increased coverage, supporting functional discovery in genome-wide experimental datasets. *Nucleic Acids Res*. 2019;**47**(D1):D607-D613.
38. Bindea G, Mlecnik B, Hackl H, et al. ClueGO: a Cytoscape plug-in to decipher functionally grouped gene ontology and pathway annotation networks. *Bioinformatics*. 2009;**25**(8):1091-1093.
39. Jassal B, Matthews L, Viteri G, et al. The reactome pathway knowledgebase. *Nucleic Acids Res*. 2020;**48**(D1):D498-D503.
40. Almagro Armenteros JJ, Tsirigos KD, Sønderby CK, et al. SignalP 5.0 improves signal peptide predictions using deep neural networks. *Nat Biotechnol*. 2019;**37**(4):420-423.
41. Kraunsøe R, Boushel R, Hansen CN, et al. Mitochondrial respiration in subcutaneous and visceral adipose tissue from patients with morbid obesity. *J Physiol*. 2010;**588**(Pt 12):2023-2032.
42. Pérez-Pérez R, Ortega-Delgado FJ, García-Santos E, et al. Differential proteomics of omental and subcutaneous adipose tissue reflects their unalike biochemical and metabolic properties. *J Proteome Res*. 2009;**8**(4):1682-1693.
43. Fischer B, Schöttl T, Schempp C, et al. Inverse relationship between body mass index and mitochondrial oxidative phosphorylation capacity in human subcutaneous adipocytes. *Am J Physiol Endocrinol Metab*. 2015;**309**(4):E380-E387.

44. Wessels B, Honecker J, Schöttl T, et al. Adipose mitochondrial respiratory capacity in obesity is impaired independently of glycemic status of tissue donors. *Obesity (Silver Spring)*. 2019;**27**(5):756-766.
45. Schöttl T, Pachl F, Giesbertz P, et al. Proteomic and metabolite profiling reveals profound structural and metabolic reorganization of adipocyte mitochondria in obesity. *Obesity (Silver Spring)*. 2020;**28**(3):590-600.
46. Keuper M, Jastroch M, Yi CX, et al. Spare mitochondrial respiratory capacity permits human adipocytes to maintain ATP homeostasis under hypoglycemic conditions. *FASEB J*. 2014;**28**(2):761-770.
47. Gealekman O, Guseva N, Hartigan C, et al. Depot-specific differences and insufficient subcutaneous adipose tissue angiogenesis in human obesity. *Circulation*. 2011;**123**(2):186-194.
48. Dadson P, Landini L, Helmiö M, et al. Effect of bariatric surgery on adipose tissue glucose metabolism in different depots in patients with or without type 2 diabetes. *Diabetes Care*. 2016;**39**(2):292-299.
49. Boden G, Merali S. Measurement of the increase in endoplasmic reticulum stress-related proteins and genes in adipose tissue of obese, insulin-resistant individuals. *Methods Enzymol*. 2011;**489**:67-82.
50. Xie X, Yi Z, Bowen B, et al. Characterization of the human adipocyte proteome and reproducibility of protein abundance by one-dimensional gel electrophoresis and HPLC-ESI-MS/MS. *J Proteome Res*. 2010;**9**(9):4521-4534.
51. Kozlov G, Gehring K. Calnexin cycle—structural features of the ER chaperone system. *FEBS J*. 2020;**287**(20):4322-4340.
52. Gurkan C, Lapp H, Alory C, Su AI, Hogenesch JB, Balch WE. Large-scale profiling of Rab GTPase trafficking networks: the membrome. *Mol Biol Cell*. 2005;**16**(8):3847-3864.
53. Li C, Yu SS. Rab proteins as regulators of lipid droplet formation and lipolysis. *Cell Biol Int*. 2016;**40**(10):1026-1032.
54. Kaddai V, Le Marchand-Brustel Y, Cormont M. Rab proteins in endocytosis and Glut4 trafficking. *Acta Physiol (Oxf)*. 2008;**192**(1):75-88.
55. Dominiczak MH, Caslake MJ. Apolipoproteins: metabolic role and clinical biochemistry applications. *Ann Clin Biochem*. 2011;**48**(Pt 6):498-515.
56. Huang ZH, Espiritu DJ, Uy A, Holterman AX, Vitello J, Mazzone T. Adipose tissue depot-specific differences in adipocyte apolipoprotein E expression. *Metabolism*. 2011;**60**(12):1692-1701.
57. Clemente-Postigo M, Queipo-Ortuño MI, Fernandez-Garcia D, Gomez-Huelgas R, Tinahones FJ, Cardona F. Adipose tissue gene expression of factors related to lipid processing in obesity. *PLoS One*. 2011;**6**(9):e24783.
58. Langeveld M, Aerts JM. Glycosphingolipids and insulin resistance. *Prog Lipid Res*. 2009;**48**(3-4):196-205.
59. Ruiz-Ojeda FJ, Méndez-Gutiérrez A, Aguilera CM, Plaza-Díaz J. Extracellular matrix remodeling of adipose tissue in obesity and metabolic diseases. *Int J Mol Sci*. 2019;**20**(19):4888.
60. Roca-Rivada A, Bravo SB, Pérez-Sotelo D, et al. CILAIR-based secretome analysis of obese visceral and subcutaneous adipose tissues reveals distinctive ECM remodeling and inflammation mediators. *Sci Rep*. 2015;**5**:12214.
61. Bertola A, Deveaux V, Bonnafous S, et al. Elevated expression of osteopontin may be related to adipose tissue macrophage accumulation and liver steatosis in morbid obesity. *Diabetes*. 2009;**58**(1):125-133.
62. Liu LF, Kodama K, Wei K, et al. The receptor CD44 is associated with systemic insulin resistance and proinflammatory macrophages in human adipose tissue. *Diabetologia*. 2015;**58**(7):1579-1586.
63. Petrus P, Fernandez TL, Kwon MM, et al. Specific loss of adipocyte CD248 improves metabolic health via reduced white adipose tissue hypoxia, fibrosis and inflammation. *EBioMedicine*. 2019;**44**:489-501.
64. Insenser M, Montes-Nieto R, Vilarrasa N, et al. A nontargeted proteomic approach to the study of visceral and subcutaneous adipose tissue in human obesity. *Mol Cell Endocrinol*. 2012;**363**(1-2):10-19.
65. Pessentheiner AR, Ducasa GM, Gordts PLSM. Proteoglycans in obesity-associated metabolic dysfunction and meta-inflammation. *Front Immunol*. 2020;**11**:1–18.
66. Lim JM, Wollaston-Hayden EE, Teo CF, Hausman D, Wells L. Quantitative secretome and glycome of primary human adipocytes during insulin resistance. *Clin Proteomics*. 2014;**11**(1):20.
67. Kochkodan J, Telem DA, Ghaferi AA. Physiologic and psychological gender differences in bariatric surgery. *Surg Endosc*. 2018;**32**(3):1382-1388.